NOVEMBER 1978 PPPL-1491
UC-20f

PLT NEUTRAL BEAM HEATING RESULTS

PLASMA PHYSICS LABORATORY

PRINCETON UNIVERSITY
PRINCETON, NEW JERSEY

This work was supported by the U. S. Department of Energy Contract No. EY-76-C-02-3073. Reproduction, translation, publication, use and disposal, in whole or in part, by or for the United States Government is permitted.

[redacted]

[illegible]

[illegible] Laboratory, Princeton University,
Princeton, New Jersey [illegible], USA

ABSTRACT

[illegible] from high-power neutral beam injection experiments on the PLT (Princeton Large Torus) tokamak at [illegible] beam power (2.4 MW) and low [illegible] [illegible] electron heating of [illegible] consistent with the [illegible] confinement [illegible] heated plasma, [illegible]

* This work was supported by the U.S. Department of Energy Contract [illegible].

Permanent Address: Department of Physics and Astronomy, University of Maryland, College Park, Maryland [illegible], USA.

+ On leave from: Centre d'Etudes Nucléaires de Fontenay-aux-Roses [illegible], B.P. No. 6, Fontenay-aux-Roses, France.

** Consultant. With Exxon Nuclear Company, Bellevue, Washington.

++ Consultant. With Westinghouse Electric Company, Fusion Power Systems Division, Pittsburgh, Pennsylvania.

1. INTRODUCTION

The purpose of the PLT (Princeton Large Torus) neutral beam injection experiment is to produce collisionless high-temperature tokamak plasmas in which to study ion and electron thermal transport. Previous neutral beam injection experiments on the CLEO [1], ATC [2], ORMAK [3], TFR [4], DITE [5], and T-11 [6] tokamaks have demonstrated substantial ion heating, bringing the ion thermal component from the plateau regime of neoclassical theory to the edge of the banana regime. Experiments on the TFR, ORMAK, and DITE tokamaks have also shown significant increases in electron temperature, but the interpretation of these results is to some degree complicated by possible changes in equilibrium or in the efficacy of ohmic heating due to changes in the concentration of low-Z impurities.

In this paper we present the results of neutral beam heating experiments on the PLT tokamak, which extend these previous results to the better confinement conditions associated with large tokamaks, and to injection power levels of up to 2.1 MW. The ion temperature increase, ΔT_i, in the PLT experiments scales with beam power and electron density approximately as $P_b/(n_e)$. At the lowest densities [$n_e(0) \sim 4.5 \times 10^{13} cm^{-3}$] and maximum power, we obtain central ion temperatures, $T_i(0)$, of approximately 5.5 keV. At $Z_{eff} \simeq 3.5$, this represents an ion thermal component as deep into the banana regime as is required for many tokamak reactor designs. The ion energy confinement time of ~25 msec is consistent with preliminary computer code calculations that take into account ion-electron coupling, neoclassical transport, ion thermal convection and charge-exchange loss. However, the uncertainties in these calculations are large due to our lack of knowledge of $q(r)$, $Z_{eff}(r)$ and especially $n_o(r)$.

Substantial electron heating has also been observed on PLT. Through the use of water-cooled graphite limiters and extensive titanium gettering, we have been able to control both the influx of high-Z impurities and the electron density increase during neutral injection. Under these circumstances, the electron temperature rises by approximately 50% to a maximum of ~3.5 keV. The volume integrated net electron energy confinement time is unchanged during injection, but the electron thermal transport in the central region of the plasma is reduced. The local net electron energy confinement time in the hot core of the discharge appears to rise well above its preinjection value.

We have also investigated certain other aspects of the neutral beam heating process. The slowing-down beam ion distribution has been measured as a function of time, energy and angle, and it exhibits good agreement with classical theory, as in previous injection experiments [1,2,3,4,5]. In addition, toroidal plasma rotation speeds of $\sim 1 \times 10^7$ cm/sec have been observed with unbalanced tangential injection, both through X-ray measurements of the Doppler shift of $m = 1/n = 1$ modes and by tangential charge-exchange measurements. The toroidal momentum input appears to be confined for a time comparable to the ion energy containment time. Finally, using 2 mm microwave scattering techniques, we have observed the onset of enhanced density fluctuations in the plasma under conditions of maximum beam power, and minimum plasma density.

The PLT neutral injection experiments have made use of a number of relatively new diagnostic techniques. Radiation measurements at ω_{ce} [7] and at $2\omega_{ce}$ [8], using microwave and far-infrared techniques, respectively,

have proved invaluable for measuring the time dependent electron-temperature profile $T_e(r)$, once the instruments have been calibrated against the multi-point Thomson scattering system [9]. X-ray crystal spectroscopy [10] of the Doppler broadened Kα radiation from Fe XXV and ultraviolet spectroscopy [11] of Doppler broadened Fe XX and Fe XXIV radiation have provided important new ion temperature measurements, as has a mass and energy analyzing charge-exchange system. A scanning bolometer has provided information on the radial profile of radiated power [12], which is necessary for understanding electron thermal transport. Without these newly developed techniques, it would have been extremely difficult, if not impossible, to provide adequate diagnosis of the neutral beam heated PLT plasma.

2. NEUTRAL BEAM OPERATION

The PLT neutral beam injection system consists of four beam lines and ion sources designed and maufactured by the Fusion Energy Division of the Oak Ridge National Laboratory (ORNL) [13]. Three of the ion sources have 22 cm diameter extraction grids and one has a 20 cm diameter grid. Each operates near the nominal voltage of 40 kV. Two sources inject parallel to the plasma current (co-injectors) and two inject anti-parallel (counter-injectors) (Fig. 1). The entrance aperture into PLT is 20 by 25 cm at 375 cm from the source grids, and permits an optimum input neutral beam power of 400-500 kW of H^0 per injector, under present conditions. With deuterium as the source gas, the neutralization efficiency is improved, and the optimum beam power rises to ~600 kW per injector.

Each injector system has magnetic deflection to remove the unneutralized fraction of the beam and deposit it onto water-cooled beam dumps. The injector systems are cryogenically pumped by condensation onto LHe cooled surfaces at 4.2° K; the effective pumping area per injector is about 3 m^2. With the transparency of the nitrogen-cooled chevron shields, this results in a pumping speed of 10 liters/sec · cm^2, or a total of 3×10^5 liters/sec per injector. For the total gas input of approximately 30 Torr · liter/sec, the pressure in the main pumping box remains at $\lesssim 10^{-4}$ Torr.

The conductance of the drift-tube which connects the main pump region to the PLT torus is limited by the restrictions imposed by the toroidal and poloidal coils and their supports. As a result, considerable beam power impinges on the drift tube walls and gives rise to a pressure increase in this region, in addition to that which occurs simply from streaming cold gas. The beam-related part of the pressure increase has been identified, from its time behavior, as probably being due to thermal degassing of the drift tube walls caused by the impinging neutral beam. The incremental pressure rise due to the beam is approximately linear in time, up to pulse lengths of 300 msec. It is essentially unaltered by the presence of the PLT fringe fields. For the usual 100 msec pulses used on PLT, the incremental pressure increase is about 30%, and the resulting product of gas pressure times path length causes $\lesssim$10% of the total throughput neutral beam power to be lost by collisional reionization and deflection in the PLT magnetic fields. We have observed that titanium gettering of the drift tube walls reduces the thermal degassing by some 30-40% for a 100 msec beam pulse, and we have recently incorporated titanium gettering into the PLT drift tubes.

3. ION HEATING

The techniques for measuring ion temperature on PLT fall into three categories: charge-exchange measurements, measurements of the Doppler broadening of impurity line radiation, and neutron emission measurements. This multiplicity of methods for determining the ion temperature is desirable because each technique has intrinsic uncertainties, and the agreement between the different measurements increases our confidence in them.

In order to improve the charge-exchange determination of ion temperature during neutral injection, a five-channel mass and energy analyzing neutral particle detector has been installed on PLT. With this device, it is possible to follow the evolution of the bulk ion distribution function without contamination from slowing-down beam ions, so long as the hydrogen isotope used in the neutral beams is different from that of the bulk plasma. We are thus able to investigate the neutral particle flux from the bulk ion species in the energy range of 1.5 to 7 times $T_i(0)$, and thereby to provide a reliable measurement of the central ion temperature.

The principal uncertainty in this measurement arises from the possibility that the thermal ion distribution may be distorted by the presence of high-power neutral beam heating. A previous linearized calculation of this effect for the Cleo tokamak [14] indicates substantial distortion when it is extrapolated to PLT injection parameters. Our own numerical calculations, however, based on the nonlinear Fokker-Planck equation [15], indicate no significant departure from a Maxwellian distribution. The principal difference between the two analyses lies in the implied energy flows. The linearized calculation assumes that the energy which flows from the beam ions into the tail particles is then coupled only into the bulk ion distribution. It also assumes that the tail particles all have lower velocities than the beam ions. In practice, however, the tail particles thermalize among themselves (a nonlinear effect) and also participate in the thermal loss processes of ion-electron coupling, charge-exchange, and neoclassical transport. In addition, the beam coupling to bulk ions actually falls off with increasing ion energy, since particularly for D^0 injection into an H^+ plasma, H^+ tail ions with $E \gtrsim 10$ keV are traveling at higher velocities than the average beam ion. The tail distortion in the linearized calculation arises more from the energy dependence of the assumed loss process (coupling to colder bulk ions $\propto 1/v^3$) than from the neutral beam heating process. When the nonlinear calculation balances neutral beam heating against the more energy independent loss processes of charge-exchange and ion-electron coupling, the bulk ion distribution is able to thermalize with itself and very little distortion develops. Thus we believe that the charge-exchange measurements reflect the true central bulk ion temperature. Figure 2 shows the time evolution of the ion temperature deduced from charge exchange for 150 msec injection of 1.6 MW of H^0 into a D^+ plasma at $\bar{n}_e = 2.2 \times 10^{13}$ cm^{-3}. Figure 3 shows a plot of fast neutral flux versus energy.

The second technique for determining the central ion temperature is to measure the neutron flux from the thermal distribution in the case of H^0 injection into a D^+ plasma. This measurement suffers from the same problem of a potentially distorted bulk ion distribution function as does the charge-exchange measurement. Again nonlinear numerical calculations [16], in this case also including large-angle or "knock on" collisions, indicate a negligible effect on the inferred ion temperature. A more serious problem, however, arises from the unknown plasma composition in

the case of high power H^0 injection into a low density D^+ plasma, where even with gettering the density rises by a factor of ~2 during injection. In these cases, although the total density increase is ~50 percent greater than the fast particle influx, the density increase on axis can be more than accounted for by the injected ions. In order to study the plasma composition in the neutron-emitting core of the discharge under conditions of high-power injection, we have performed the opposite injection scenario: D^0 injection into an H^+ plasma. By measuring the neutron emission from the thermal plasma after the beam pulse is turned off and the fast ions have thermalized, and also knowing the ion temperature during this period from other diagnostics, we are able to estimate the increase in deuterium density on axis. By this means we have determined that the density increase in the center of the plasma does indeed correspond approximately to the density increase due to the injected beam species. The uncertainty in this measurement of the plasma composition, however, results in rather large error bars for T_i (~800 eV) in the case of H^0 injection into low-density D^+ plasmas. Figure 4 shows the neutron-deduced ion temperature versus time for a case of 1.6 MW injection of H^0 into a D^+ plasma at $\bar{n}_e = 2.2 \times 10^{13}$ cm^{-3}, as in Fig. 2. In this case, however, the beam pulse length was 100 msec.

The third technique for determining the ion temperature is by Doppler broadening measurements. Two new approaches have been developed for measuring line widths from highly-ionized states of iron. In the first approach, a forbidden line of Fe XX has been identified at 2665.1 Å, and its Doppler width is used as a diagnostic for the near-central ion temperature, since experimentally the peak of the Fe XX radiation is found at $r \lesssim 10$ cm even in discharges with $T_e(0) = 3$ keV. Figure 5(a) shows a representative line width from a 2.1 MW $D^0 \rightarrow H^+$ injection case. At the highest ion temperatures we are also able to use ultraviolet radiation from Fe XXIV for Doppler broadening measurements more nearly at the center of the plasma. Figure 5(b) shows a representative line width from a similar case to that of Fig. 5(a). Figure 6 shows $T_i(t)$ from Fe XX for a case similar to that of Fig. 4. In another approach, a high resolution ($E/\Delta E$ = 15000) X-ray crystal spectrometer is used for line broadening measurements of the 1s - 2p Kα transition of the heliumlike state of iron, Fe XXV, at 1.85 Å. The spectrometer consists of a curved quartz crystal and a multiwire proportional counter in the Johann configuration. Radiation from the 1s - 2p transition should be emitted from a narrow region in the hot core of the plasma for central electron temperatures in the range from 1.2 keV to 6 keV. Figures 7(a) and 7(b) show the line widths, and Fig. 8, $T_i(t)$ for a case similar to that of Fig. 2. The arrows in Fig. 7 indicate the limits of the range used for a least squares fit of the experimental data to a Voigtian (the convolution of the Gaussian due to Doppler broadening with the narrow Lorentzian profile due to the natural line width). The limits are chosen to exclude small satellite lines on the long wavelength side.

The Doppler broadening measurements do not suffer from the same uncertainties with respect to the distortion of the bulk ion distribution function as do the neutron and charge-exchange measurements, however, the impurity ion temperature may not be precisely equal to the temperature of the bulk ion species. The power coupled from the beam ions to each ion species in the plasma is proportional to $n_i Z_i^2/m_i$. Thus, while the total power delivered to impurity ions may be small, the power per ion scales as Z_i^2/m_i. At low densities and high ion temperatures, the impurity-hydrogen coupling time becomes long enough so that a temperature difference should develop

between the impurity ions and the hydrogenic species. For our low density cases where $Z_{eff} \approx 3$, due primarily to carbon, all of the impurity ions are well coupled to each other, and one may write a simple equation governing the impurity temperature, T_x:

$$\frac{dT_x}{dt} = 0 = \frac{T_H - T_x}{\tau_{x-H}} + \left.\frac{dT_x}{dt}\right|_{beam} + \frac{T_e - T_x}{\tau_{x-e}} - \frac{T_x}{\tau_{Ex}}$$

where τ_{x-H} and τ_{x-e} are the energy equilibration times [17] between the impurities and the hydrogenic species, and between the impurities and the electrons, respectively. τ_{Ex} is the energy containment time of the impurities. If we take the dominant impurity to be carbon, and solve this equation for a case of 2.1 MW D^0 injection into a low density initially H^+ plasma, where $T_H = 5.0$ keV, $T_e = 3.2$ keV, $n_e = 4.5 \times 10^{13}$ cm^{-3}, the mean atomic mass $A_H = 1.5$, $n_H = 2.3 \times 10^{13}$ cm^{-3}, $\left.dT_x/dt\right|_{beam} = 8.6 \times 10^5$ eV/sec, from the Monte-Carlo code described below, and (estimating) $\tau_{Ex} = 20$ msec, we arrive at $\tau_{x-H} = 1.7$ msec, $\tau_{x-e} = 25$ msec and $T_x - T_H = 800$ eV. This evaluation of $T_x - T_H$, unfortunately, is uncertain to within a factor of 2; the possible temperature differential drops dramatically, however, as the density increases, and especially as the ion temperature decreases. For the 4 keV, slightly higher density cases of 1.6 MW H^0 injection into D^+ plasmas, this effect is within the experimental accuracy of the measurements.

The Doppler-broadening measurements are extended to light impurities in addition to iron, in order to produce a radial profile of the ion temperature. Figure 9 shows the ion temperature profile before and during injection for the same case as in Figs. 2 and 7. The radial positions of C III and C V were measured using a fast scanning mirror, and the position of O VII was determined from the measured $T_e(r)$ and $n_e(r)$ profiles coupled to an oxygen diffusion calculation [17]. The location of Fe XX was deduced from radial scans of vacuum ultraviolet (VUV) emission from Fe XXI and Fe XXII, which should be located close to Fe XX.

Figure 10 shows the results from our first runs with four neutral beams, carbon limiters and titanium gettering. The charge-exchange data points are plotted without the small positive correction needed to deduce $T_i(0)$, and the Fe XX Doppler broadening measurements reflect T_i at $r \approx 7.5$ cm, not on axis. In view of the steep gradient of $T_i(r)$, the Fe XX temperature might have been expected to lie below the charge-exchange $T_i(0)$; this spatial differential in T_i, however, is roughly compensated by the difference between the hydrogen and impurity temperatures, which has been described above. In general, the good correlation between the different measurements indicates that the deduced ion temperatures are reliable. Figure 11 shows a log plot of the same data as that in Fig. 10, but here in terms of the heating effectiveness, $\Delta T_i/P_b$ in eV/kW versus the line average electron density at the end of the injection pulse. The heating effectiveness scales approximately as $(\bar{n}_e)^{-1}$, consistent with the results of other neutral injection experiments on ORMAK [3] and TFR [4]. At the lowest densities and highest ion temperatures, ν_i^* is less than 10^{-1} over most of the radial profiles, so the ion thermal component is deep in the banana regime, with no evident deterioration in energy confinement. Preliminary ion energy balance calculations are discussed under "Ion and Electron Energy Balance."

PLT has also been operated with D^0 injection into a D^+ plasma in order to simulate the power multiplication anticipated in beam

driven subignition reactors. We obtain the largest neutron yields with high-power injection into hot, low density plasmas. With 1.7 MW of 35 keV D^0 beams injected into a $\bar{n}_e = 2 \times 10^{13} cm^{-3}$ plasma, we reach a maximum neutron emission of 4×10^{13} neutrons/sec. With a 200 msec beam pulse, we obtain 7×10^{12} neutrons/shot (Fig. 12). Computer code calculations [18] of the neutron production to be expected for these cases indicate a flux of 6.5×10^{13} neutrons/sec. Since there are possible variations of order 50% in the computed production rate, due to uncertainties in the input plasma parameters, such as n_D/n_e, and since there are factor-of-two uncertainties in the neutron measurement, the agreement between theory and experiment can be considered satisfactory.

At the highest beam power achieved to date (2.1 MW D^0 injection into an H^+ plasma), the average ion energy in the center of the plasma is high. From the Monte-Carlo code described below we calculate $n_b(0) = 1.2 \times 10^{13} cm^{-3}$, $\bar{E}_b(0) = 19$ keV, and we have $n_i(0) \approx 2.5 \times 10^{13} cm^{-3}$, $\bar{E}_i(0) = 8.25$ keV, so the average ion energy on axis is approximately 12 keV, and $\Gamma(0) = n_b \bar{E}_b : [(3/2) n_i T_i + (3/2) n_e T_e] = 0.7$.

4. ELECTRON HEATING

The electron heating obtained in PLT with neutral injection is very sensitive to the choice of limiter material and to the conditions of the vacuum vessel wall. In our initial experiments, using two neutral beams and a maximum beam power of 1.1 MW (August-December 1977), we employed a tungsten limiter and Taylor Discharge Cleaning (TDC) [19] to condition the walls. Under these circumstances light impurity concentrations were relatively low (Z_{eff} = 2-4), but with even modest amounts of counter-injected beam power tungsten radiation from the core of the plasma would quench any significant temperature rise. Indeed in the low density high-power cases, $T_e(0)$ fell substantially during injection. This electron behavior limited the ion temperature increase during injection to $\lesssim$1.3 keV, even in the lowest density, highest power cases. During this period we also experimented with a simple carbon limiter in the form of a solid 15 cm diameter graphite rod with a curved end touching the plasma surface. Using this limiter, the preinjection plasma was generally freer of tungsten radiation, and hotter than otherwise, but still large amounts of tungsten entered the discharge during counter-injection. The source of this tungsten may have been sputtering due to beam ions on loss orbits striking the retracted limiters and the tungsten-coated vacuum vessel wall, or it may have been due to effects associated with the increased edge ion and electron temperatures observed during counter-injection. We also experimented with limited titanium gettering on the vacuum vessel surface, and found that we were able to run stable, low Z_{eff} discharges at both higher and lower densities than without gettering, and that the density increase with neutral injection was substantially reduced.

In our more recent experimental runs with four neutral beams (June-August 1978), we have fitted PLT with interchangeable large-area ATJ graphite and stainless steel limiters. The graphite limiters, which are located top and bottom, face the plasma surface with an area of ~750 cm^2 each, and are provided with water cooling. Furthermore, PLT has been equipped with three getter balls capable of evaporating titanium on nearly the entire vacuum vessel wall.

Figures 13(a) and 13(b) show a comparison of radiated power profiles, between low power counter-injection into a steel-limiter plasma, and high

power co- and counter-injection into a plasma with graphite limiters. In case (a) $T_e(0)$ dropped by 700 eV, while in case (b) $T_e(0)$ increased. The radiation of ~0.4 W/cm^3 from the plasma periphery is relatively unimportant to the electron power balance as compared to 1 W/cm^3 from the plasma core. Clearly the carbon limiters represent a substantial improvement. With the use of extensive titanium gettering, we have also been able to limit the density increase to $\Delta\bar{n}_e = 1 \times 10^{13}$cm^{-3} with four beam injection into a plasma which starts at $\bar{n}_e = 1 \times 10^{13}$cm^{-3}. At higher densities ($\bar{n}_e \gtrsim 2.5 \times 10^{13}$ cm^{-3}) we are able to hold the density nearly constant during injection, through feedback control of the pulse valve gas feed. In addition, gettering results in a decreased Z_{eff} and a wider operating range in density [19].

Figure 14 shows laser scans of a high density plasma before and during injection of 1.2 MW $H^0 \rightarrow D^+$. With the feedback density control, $n_e(r)$ is almost unchanged, and T_e rises by nearly 50% over the entire profile. Z_{eff} is constant at approximately 1.5. The time dependence of the electron temperature in these discharges, measured from the far-infrared emission at $2\omega_{ce}$, is shown in Fig. 15. The instrument used to make these measurements was a grating polychromator coupled to a Putley detector. The large amplitude (ΔT_e ~ 300 eV), long period sawteeth, which are quite visible in the central trace, are a common but not universal feature of high-power injection. The time dependence of this heating, especially the return to the initial baseline, is a characteristic signature of discharges where the impurity concentrations remain unchanged. In cases with metallic limiters, where strong central core radiation comes up during injection, the electron temperature returns to a value below that of preinjection. At low densities, with D^0 injection into H^+ plasmas, we have also been able to achieve substantial electron heating. In these cases Z_{eff} is higher (3-4), and the initial electron temperature is larger. Figure 16 shows radial profiles of $T_e(r)$ for a case of 2.1 MW D^0 injection into a low density H^+ plasma. At the end of the injection pulse, $\bar{n}_e$ is 2.3×10^{13}cm^{-3} and $n_e(0)$ is 4.5×10^{13}cm^{-3}. In this case $T_e(r)$ was deduced from a swept measurement of the microwave emission at ω_{ce}. An interesting and important feature of all these measurements is that the $T_e(r)$ profile shape changes very little during injection.

Figure 17 shows a compilation of the results of high power injection into gettered carbon limiter plasmas. The cases of H^0 injection into low density D^+ plasmas which show little heating are generally characterized by relatively large density increases, probably due to the less extensive gettering in these cases. The overall picture, however, suggests that under the best conditions $\Delta T_e/P_b \approx 0.6$ eV/kW, independent of plasma density. Qualitatively, this result is consistent with the empirical scaling law $\tau_{Ee} \propto n_e$.

5. ION AND ELECTRON POWER BALANCE

In order to develop a preliminary understanding of the significance of these results, we have performed numerical calculations of the ion and electron radial power flows both with and without neutral injection. For simplicity, these calculations are time independent, and so are only valid for the period of quasi-equilibrium temperature and density near the end of the neutral beam pulse, or for a period of quasi-equilibrium in the ohmic heating phase of a discharge. Figure 18 shows the logical structure of our calculations. Radial profiles of $n_e(r)$ from the Thomson scattering

system and of $T_e(r)$ from Thomson scattering, ω_{ce} or $2\omega_{ce}$ measurements are used as the basic input parameters. These are passed to a Monte-Carlo beam-orbit calculation [20] which follows the orbits and slowing down of 500 fast ions and calculates the power given to the bulk ions, P_{bi}, and to the electrons, P_{be}. It also calculates the energy lost by charge-exchange of beam ions on background neutrals and by fast ions scattered onto loss orbits. An important effect which is included in this code, and not in most other such calculations, is the possibility that fast ions which charge-exchange and start to leave the plasma often reionize before they escape. From the measurements of T_i, we estimate a $T_i(r)$ on the basis of neoclassical thermal conduction, ion-electron coupling, empirical thermal convection and charge-exchange loss, as in Ref. [22]. In general, we find that the uncertainties in $Z_{eff}(r)$, $q(r)$, and $n_o(r)$ result in a rather large range of possible prediction from this series of calculations. The neutral density profile, $n_o(r)$, which is important for the low density cases, has been calculated using a highly simplified model [23]. On the other hand, even the most sophisticated models for $n_o(r)$ do not properly treat the case where $n_b/n_e \sim 0.25$, and so the beam ions themselves participate strongly in the charge-exchange transport of neutrals across the plasma column. With these caveats in mind, we vary the unknown parameters over a reasonable range, and find the resulting range of the classical prediction of the ion temperature. In order to now proceed with the electron power flow calculation and also to determine τ_{Ei}, we finally fix on a choice of parameters which gives good agreement with the experimental data.

Figure 20 shows the ion temperature profile which results from this procedure for a case of 2.1 MW D^0 injection into a low density [$n_e(0) = 4.5 \times 10^{13} cm^{-3}$] H^+ plasma; the experimentally measured profile is also plotted. The iron Doppler broadening measurement points have the estimated 800 eV differential between T_x and T_H subtracted off in this case. The errors on the calculated $T_i(r)$ curve indicate that the range of prediction for this case varied from 4 keV to approximately 7.5 keV. The errors on the individual measurements are ±10%. Figure 21 shows the calculated ion collisionality, ν_i^*, versus radius, including the effect of collisions with impurities. The volume integrated net ion energy confinement time, defined as

$$\frac{\int (3/2) n_i k T_i \, d^3r}{(P_{bi} - P_{ic})}$$

is 25 msec for the best fit to the experimental data. In the ohmically heated phase of this same discharge, well after the end of injection, the net ion energy confinement time, defined as

$$\frac{\int (3/2) n_i k T_i \, d^3r}{P_{ei}}$$

is ~50 msec. In the calculation, this difference is mostly due to the enhanced role of charge-exchange loss at high ion temperatures and steep temperature gradients. Indeed the "best case" calculation, where T_i rises to 7.5 keV on axis, only shows a net ion energy confinement time of 30 msec. Thus the reduction in τ_{Ei} is consistent with our classical model. On the other hand, because neoclassical transport is only a small fraction of the total energy flow in this case, we cannot rule out as much as a 5 fold enhancement of the ion thermal conduction over the neoclassical value. Our knowledge of the true neoclassical value is itself uncertain by nearly as large a factor, due to the uncertainty in the experimental values of $Z_{eff}(r)$ and $q(r)$.

In cases of neutral injection into higher density plasmas, charge exchange plays a much smaller role, and electron-ion coupling (which we can accurately calculate) becomes the dominant term in the ion energy flow. Neoclassical thermal conduction is again a small part of the transport, in part because Z_{eff} is low. Figure 22 shows the calculated ion temperature profile for a case of 2.0 MW D^0 injection into an H^+ plasma with $\bar{n}_e = 3.5 \times 10^{13}$ cm^{-3} and $n_e(0) = 7.5 \times 10^{13}$ cm^{-3}. Again the error bar represents the range of classical prediction. The errors in the experimental ion temperature measurement have increased to ±15% in this case, due to the reduced iron radiation and charge-exchange flux at higher densities. The calculated net ion energy confinement time is 95 msec, which compares well with the net ion energy confinement time of ≤120 msec in the post-injection Ohmic phase of the same discharge. In this beam-heated case, as in the low density case, the ions are in the banana regime over almost the entire radial profile, although here the minimum ν_i^* is ~8×10^{-2}. As noted above, neoclassical transport is masked by ion-electron coupling, and with the scatter of our data, the maximum credible enhancement over neoclassical ion thermal conduction could be a factor of 3-4.

On the basis of these ion power flow calculations, which have been calibrated against the experimental data, we can now proceed to examine the electron power flows. From the Monte-Carlo beam-orbit code we have the radial profile of P_{be}, the power flowing from the beam ions to the electrons, and from the ion neoclassical calculation we have the profile of P_{ie}, the power flowing from the bulk ions to the electrons. An additional term which is important at low densities is P_{ne}, the power required to thermalize the cold electrons which enter the plasma with the beam ions; this is calculated by the beam-orbit code. The ohmic heating input power is calculated from the experimental $T_e(r)$ profile, assuming $Z_{eff}(r) = \text{const.}$, and $\sigma \propto T_e^{3/2}$. It is difficult to measure the resistive component of the loop voltage during injection because as the electron temperature increases, V_{Loop} drops, but I_p also increases by 20-40 kA, causing a significant inductive contribution to V_{Loop}. As best we can determine, ±25%, the plasma conductivity scales as $T_e^{3/2}$ when the temperature increases due to neutral injection. Therefore we use the assumption of constant Z_{eff} to calculate the resistive component of the loop voltage during injection from V_{Loop} during the quasi-equilibrium period before injection. Because the electron temperature profile shape changes little during injection, we ignore the effects of any variation in the internal inductance.

In the low density case considered above, the ion power balance calculations indicated that 300 kW of power was being emitted from the plasma by charge exchange of the thermal ions, while the bolometer measurement indicated a total output power of 1 MW, slightly greater than the total

calculated input power to the electrons. In an attempt to subtract off the effect of charge exchange neutrals on the bolometer, we have simply scaled P_{rad} by 0.7 from the bolometrically measured emission. The resulting radiated power is consistent with the spectroscopically estimated radiation of ~200 mW/cm^3 in this case. Note that the contribution to the bolometer signal from charge-exchange beam ions may be small, since they are emitted from the plasma mostly tangentially, and the bolometer has a collimated perpendicular view.

Figure 23 shows the resulting electron power flows. The only term not previously described is P_{con}, the power carried by conduction and convection, which must be equal to the sum of the other terms, under the assumption of steady-state conditions. It is interesting to note that in the core region of the plasma, the net beam input power, $P_{be} + P_{ei} - P_{ne}$ is still less than P_{OH}, although P_{OH} has dropped from 750 kW in the ohmic heating case to 500 kW in the beam heated case.

Figure 24 shows the radially integrated net τ_{Ee} for the low density beam heated case, where $\tau_{Ee}(r)$ is defined as

$$\frac{\int_0^r (3/2) n_e k T_e \, d^3r}{(P_{OH} + P_{be} + P_{ie} - P_{ne} - P_{rad})} .$$

On this figure, we also plot the net $\tau_{Ee}(r)$ for the same discharge in the ohmically heated plasma well after injection. The central electron density in this case has dropped by 40% after injection, but $\bar{n}_e$ is approximately constant. The definition of $\tau_{Ee}(r)$ for the ohmically heated case is

$$\frac{\int_0^r (3/2) n_e k T_e \, d^3r}{(P_{OH} - P_{ei} - P_{rad})} .$$

Within the accuracy of these calculations (±30-40%) the volume integrated net τ_{Ee} is unchanged during injection, but the energy confinement in the core of the plasma appears substantially enhanced. The beam heating and ion-electron coupling in the center of the plasma is weak due to the high electron temperature, and yet the central temperature rises proportionally to the temperature half-way out, where much more beam power and ion-electron coupling power is deposited. Had the electron thermal conduction coefficient remained unchanged during injection, one would have expected a broadening of the T_e profile, and a reduction in the net τ_{Ee}. The experimental results, by contrast, indicate a substantial reduction in χ_e in the hot central region of the discharge, as shown in Fig. 25. Here $\chi_e(r)$ is defined as

$$\chi_e = \frac{P_{con}}{4\pi^2 R_o r n_e \, dT_e/dr} .$$

If we calculate a gross $\tau_{Ee}(a)$ for these cases, where we do not subtract off P_{rad}, we find that both cases have $\tau_{Ee}(a) = 14$ msec, a typical gross electron energy confinement time for low density gettered PLT discharges.

An interesting feature of these low density discharges is the substantial energy required to heat the cold electrons that enter the core of the plasma with the beam ions. Experimentally, at low densities we generally see a dip in $T_e(0)$ at the start of injection, and a significant increase (~10%) during a 30 msec period after the beam is shut off. This behavior is consistent with the fact that P_{ne} turns on and off sharply with the beam pulse, while P_{be} and P_{ei} require 30-50 msec to build up and to decay. Figure 16 shows radial scans of T_e from ω_{ce} radiation which demonstrate the late rise quite clearly. Note that most of the post-injection temperature rise occurs near the center of the discharge, where P_{ne} is relatively most important.

When we perform these same calculations for the higher density plasma ($\bar{n}_e = 3.5 \times 10^{13}$ cm^{-3}) we obtain a similar result. Figure 26 shows the power flows for this case. The radiated power is now a smaller fraction of the total power balance (and should not be significantly affected by charge exchange), and P_{ie} is substantially increased at the higher density, while P_{ne} becomes negligible. The net $\tau_{Ee}(r)$ for the beam heated plasma and for the ohmically heated plasma later in the same discharge is shown in Fig. 27. The density profiles in the two cases are very similar. Again, to within the accuracy of this calculation, the volume integrated τ_{Ee} is effectively unchanged, but the electron thermal transport in the core of the plasma is significantly reduced. In this case, the gross $\tau_{Ee}(a)$ for the ohmically heated plasma was 19 msec, and for the beam heated plasma, 17 msec.

We are not in a position at this point to speculate on a possible cause for the enhanced confinement properties of the electrons in the core of the discharge during neutral injection, but despite the limited accuracy of this analysis, it does appear to be a clear effect. It seems unlikely, however, that the improved confinement is a simple scaling of χ_e with T_e, in light of the fact that the electron thermal transport was not reduced in the outer regions of the plasma, which were also heated.

6. OTHER ASPECTS OF NEUTRAL INJECTION

In addition to studying ion and electron heating on PLT, we have also investigated certain other aspects of neutral beam injection. Using a horizontally scanning fast neutral detector, we have measured the angular dependence of the fast-ion energy distribution during injection. Figure 28 shows an angle and energy spectrum for a case of 360 kW H^0 co-injection into a D^+ plasma. The theoretical curve was calculated on the basis of a numerical solution of the bounce-averaged Fokker-Planck equation [24]. It shows reasonable agreement with experiment over a range of angles from parallel to nearly perpendicular to the magnetic field. The Z_{eff} used in the numerical calculation was 2, which agrees well with the conductivity Z_{eff} of 2.5 ± 1.

We have also made preliminary fast-ion measurements in the recent high power injection runs. One of the features of the fast-ion distribution function which is most sensitive to any nonclassical behavior is the high energy beam ion tail above the injection energy [1]. Figure 29 shows this tail above E_{inj} in the counter-facing direction for a case of 2.1 MW D^0 injection into a low density H^+ plasma. The measured tail temperature of 2.7 keV agrees well with the theoretically calculated value of

2.5 keV, where the calculated temperature arises from taking into account collisions between beam ions and plasma ions and electrons, combined with the decelerating effect of the toroidal electric field.

One of the mysterious aspects of neutral injection in previous tokamak experiments has been the small rate of toroidal rotation observed in cases of unbalanced tangential injection [25]. We have begun to study this problem in PLT with two separate diagnostic techniques. In the first approach, we have used the X-ray wave detector arrays [26] to investigate the effects of unbalanced injection on the propagation of the $m = 1/n = 1$ precursor oscillations associated with internal disruptions. Without injection, the toroidal phase velocity of these oscillations is generally about -3×10^6 cm/sec, and the poloidal propagation is in the electron diamagnetic direction. As shown in Fig. 30, with co-injection of ~400 kW D^0 into a low density H^+ plasma, the toroidal phase velocity is $+1 \times 10^7$ cm/sec, and the propagation is in the ion diamagnetic direction. With almost pure counter-injection, the toroidal phase velocity is about -1.5×10^7 cm/sec, and the propagation is in the usual electron diamagnetic direction. If we interpret the change in phase velocity as a Doppler-shift due to toroidal fluid motion (since theoretically any poloidal rotation is rapidly damped) we find a rotation velocity about $\pm 1 \times 10^7$ cm/sec.

The toroidal rotation of the plasma can also be investigated using the horizontally scanning fast neutral detector, aligned in the tangential direction. Since co- and counter-injection heat the plasma ions with approximately equal effectiveness, we expect a difference in the tangential thermal charge-exchange spectrum for the two cases due solely to rotational effects. Experimentally, with the analyzer facing counter-going ions, we observe a significantly larger thermal charge-exchange flux with counter-injection than with co-injection. For a shifted Maxwellian ion distribution, the toroidal rotation speed can be derived from this experimental ratio, $R(E)$, using the formula

$$\frac{v_\phi \text{ (cm/sec)}}{T_i \text{ (keV)}} = 1.09 \times 10^7 \frac{\ln [R(E)]}{[E \text{ (keV)}\ A_p]^{1/2}}$$

where E is the energy of the charge-exchange neutral, and A_p is its atomic mass. This expression is evaluated as a function of time from the charge-exchange flux in the energy range of 3-6 keV in Fig. 31 for a case of 500 kW D^0 injection into a low density H^+ plasma. Although temperature measurements were not made in this case, $T_i \approx 1.7$-2.0 keV is expected, giving a rotation speed of $\geq 10^7$ cm/sec. Note that v_ϕ/T_i decays after injection in about 60 msec, and since T_i decays during this same period, v_ϕ must fall somewhat more rapidly.

We have also begun investigations of the stability of the PLT plasma in the ion cyclotron range of frequencies with neutral injection. Using electromagnetic pickup loops in the shadow of the limiter, we observe toroidal eigenmodes at the fundamental and first harmonic of the ion cyclotron frequency of the beam species, evaluated at $r \approx 0$, for both H^0 and D^0 injection into D^+ plasmas and for D^0 injection into H^+ plasmas. With high power injection, the waves persist only for the first 10 to 30 msec of the beam pulse and then damp out rapidly. These modes are observed to have low toroidal and poloidal mode numbers and narrow bandwidths of 1 MHz. Work is in progress to elucidate the physics of the excitation mechanism and to evaluate the energy contained in the wave.

Density fluctuations with wavelengths in the range of 0.2 to 2 cm and with a spectrum in the range of frequencies of drift waves have also been observed, using 2 mm microwave scattering techniques [27]. Under most circumstances, the scattered power level increases by ≤ 2 during injections, and the frequency spectrum is largely unchanged. At the highest power levels, however, we observe a substantial increase in the scattered radiation at some wavenumbers [Fig. 32(a)], and the frequency power spectrum shows discrete mode structure [Fig. 32(b)]. We do not yet know whether these waves are associated with the high-power injection, or with the concomitant high ion temperatures, nor are we able, as yet, to assess their importance to thermal transport, since neither their k-spectrum nor their radial profiles have been measured.

7. CONCLUSIONS

The results of the first experiments on PLT with four neutral beams, water-cooled graphite limiters, and extensive titanium gettering have been quite encouraging. At moderate densities [$n_e(0) = 7.5 \times 10^{13}$ cm^{-3}] we have achieved substantial electron and ion heating, pushing the ions well into the banana regime — with no deleterious effects on thermal transport. Indeed the central electron energy confinement appears to improve with neutral beam heating. At lower densities [$n_e(0) = 4.5 \times 10^{13}$ cm^{-3}], the ion and electron heating which results from neutral beam injection at 2.1 MW is quite dramatic and produces a high temperature, collisionless plasma. The very fact that such a plasma can be created in PLT indicates that thermal transport under these conditions does not have the strongly unfavorable temperature dependence of trapped particle modes. Much more work is required, however, to understand the confinement properties of high temperature tokamak plasmas and to evaluate the implications of these results for future research.

ACKNOWLEDGMENTS

The continuing support of Drs. M. B. Gottlieb, E. A. Frieman, and H. P. Furth is gratefully acknowledged.

The High Power Neutral Beam Injectors which made these experiments possible were developed at the Oak Ridge National Laboratory by Dr. H. H. Haselton and his group under the direction of Dr. O. B. Morgan, Jr.

The data acquisition group under Dr. F. Seibel has played an essential role in these experiments by making available sophisticated techniques for analyzing the data from many diagnostic instruments.

The authors express their appreciation to Drs. D. Post, J. Odgen, D. Jassby, and H. Towner for contributing modelling calculations and to Dr. T. Stix for his significant contributions to the early design work and expected performance evaluations.

We also wish to thank the PPL Engineering and Technical Support Groups for the tremendous effort necessary to achieve successful operation of the PLT tokamak, the neutral beam injectors, the high power supplies, and the diagnostic systems.

[1] CORDEY, J.G., et al., Nuclear Fusion 14 (1973) 441.
[2] BOL, K., et al., in Plasma Physics and Controlled Nuclear Fusion Research (Proc. 5th Int. Conf. Tokyo, 1974) Vol. I, IAEA, Vienna (1975) 77.
[3] BERRY, L.A., et al., in Plasma Physics and Controlled Nuclear Fusion Research (Proc. 6th Int. Conf. Berchtesgaden, 1976) Vol. I, IAEA, Vienna (1977) 49.
[4] EQUIP TFR, ibid., Vol. I, IAEA, Vienna (1977) 69.
[5] PAUL, J.W.M., et al., in Controlled Fusion and Plasma Physics (Proc. 8th Europ. Conf., Prague, 1977) Vol. II, 49.
[6] BLASENKOV, V.S., et al., in Plasma Physics and Controlled Nuclear Fusion Research (Proc. 6th Int. Conf. Berchtesgaden, 1976) Vol. I, IAEA, Vienna (1977) 85.
[7] ARUNASALAM, V., et al., Bull. Am. Phys. Soc. 23 (1978) 689.
[8] TAIT, G.D., BOYD, D.A., Bull. Am. Phys. Soc. 23 (1978) 688.
[9] BRETZ, N., et al., Applied Optics 17 (1978) 192.
[10] BITTER, M., et al., Bull. Am. Phys. Soc. 23 (1978) 698.
[11] SUCKEWER, S., HINNOV, E., Princeton Plasma Physics Laboratory Report 1465 (1978); to be published in Phys. Rev. Lett.
[12] HSUAN, H., et al., in Symposium on Heating in Toroidal Plasmas (Proc. Joint Varenna-Grenoble Int. Symp., Grenoble, 1978) Vol. II.
[13] KIM, J., et al., in 2nd Topical Meeting on Technology of Controlled Fusion (Proc. 2nd Topical Meeting, Richland, 1976) Vol. 4, NTIS, Springfield, Virginia (1976) 1213.
[14] CORDEY, J.G., in Plasma Physics and Controlled Nuclear Fusion Research (Proc. 5th Int. Conf. Tokyo, 1974) Vol. I, IAEA, Vienna (1975) 623.
[15] KILLEEN, J., MARX, K.D., Methods of Computational Physics 9, Ed. B. Alder, Academic Press, New Yrok (1970) 422.
[16] KULSRUD, R., SUN, Y., private communication.
[17] SUCKEWER, S., HINNOV, E., Nuclear Fusion 17 (1977) 945.
[18] STRACHAN, J.D., et al., Phys. Lett. 66A (1978) 295.
[19] BOL, K., et al., proceedings this conference, IAEA-CN-37-A-1.
[20] JASSBY, D.L., GOLDSTON, R.J., Nuclear Fusion 16 (1976) 613.
[21] BRUSATI, M., et al., Princeton Plasma Physics Laboratory Report 1403 (1977); to be published in Nuclear Fusion.
[22] STOTT, P.E., Plasma Physics 18 (1976) 251.
[23] GOLDSTON, R.J., Princeton Plasma Physics Laboratory Report 1443 (1978); to be published in Plasma Physics.
[24] CORDEY, J.G., Nuclear Fusion 16 (1976) 499.
[25] SMITH, R.R., private communication.
[26] SAUTHOFF, N.R., et al., Bull. Am. Phys. Soc. 23 (1978) 698.
[27] MAZZUCATO, E., Phys. Fluids 21 (1978) 1063.

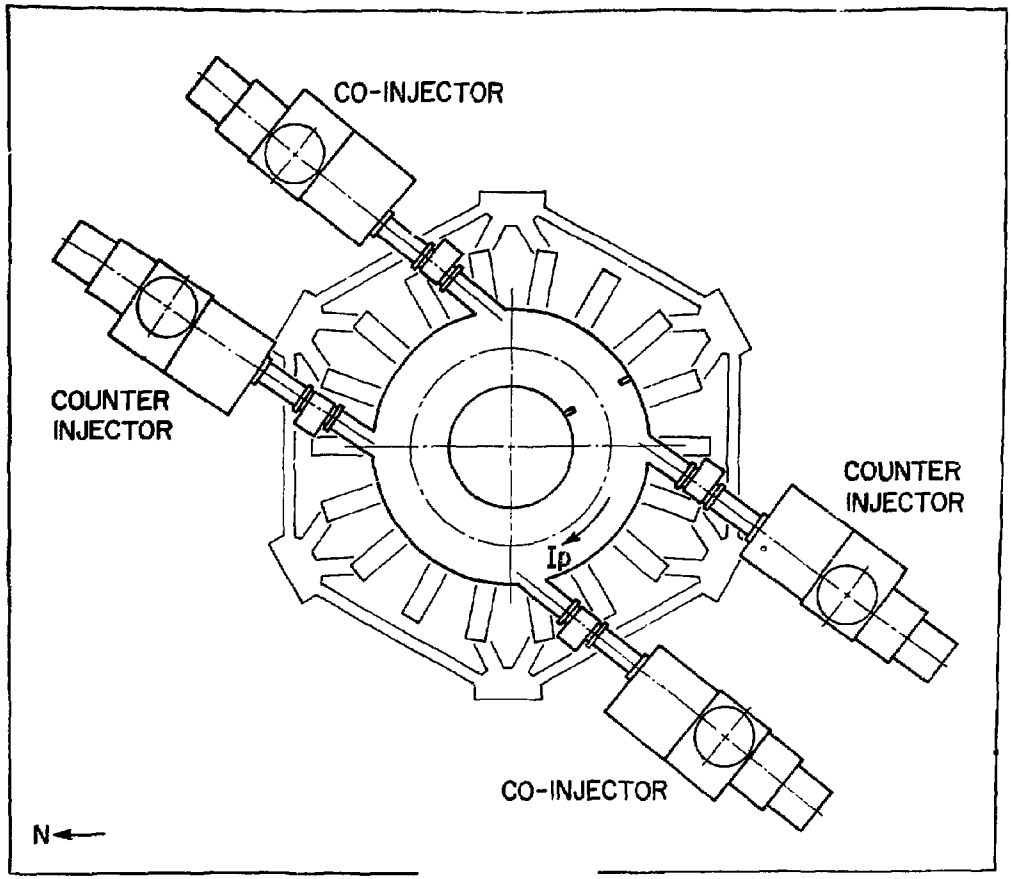

Figure 1. PLT schematic indicating the direction of the plasma current and the postion of the neutral beam injectors. (PPPL-783851)

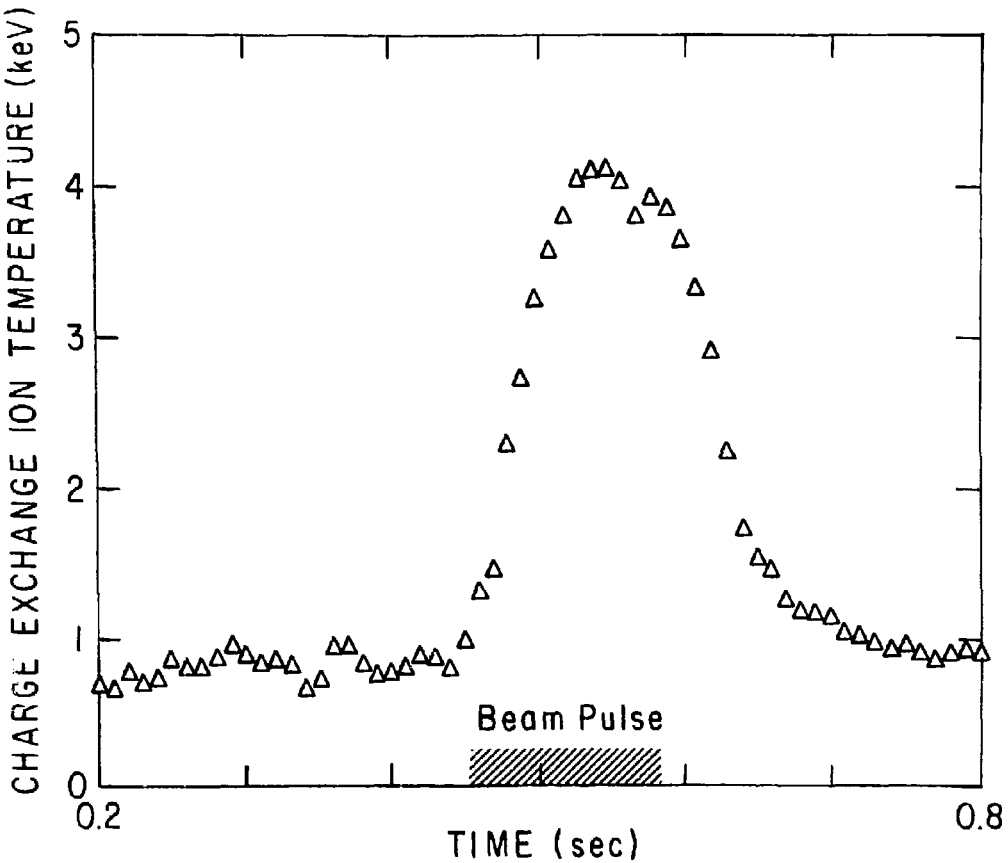

Figure 2. Charge exchange ion temperature as a function of time during the discharge. time resolution is 10 ms. A peak ion temperature of 4 keV is attained during injection of 1.6 MW of H° into a D^{+} plasma. (PPPL-783872)

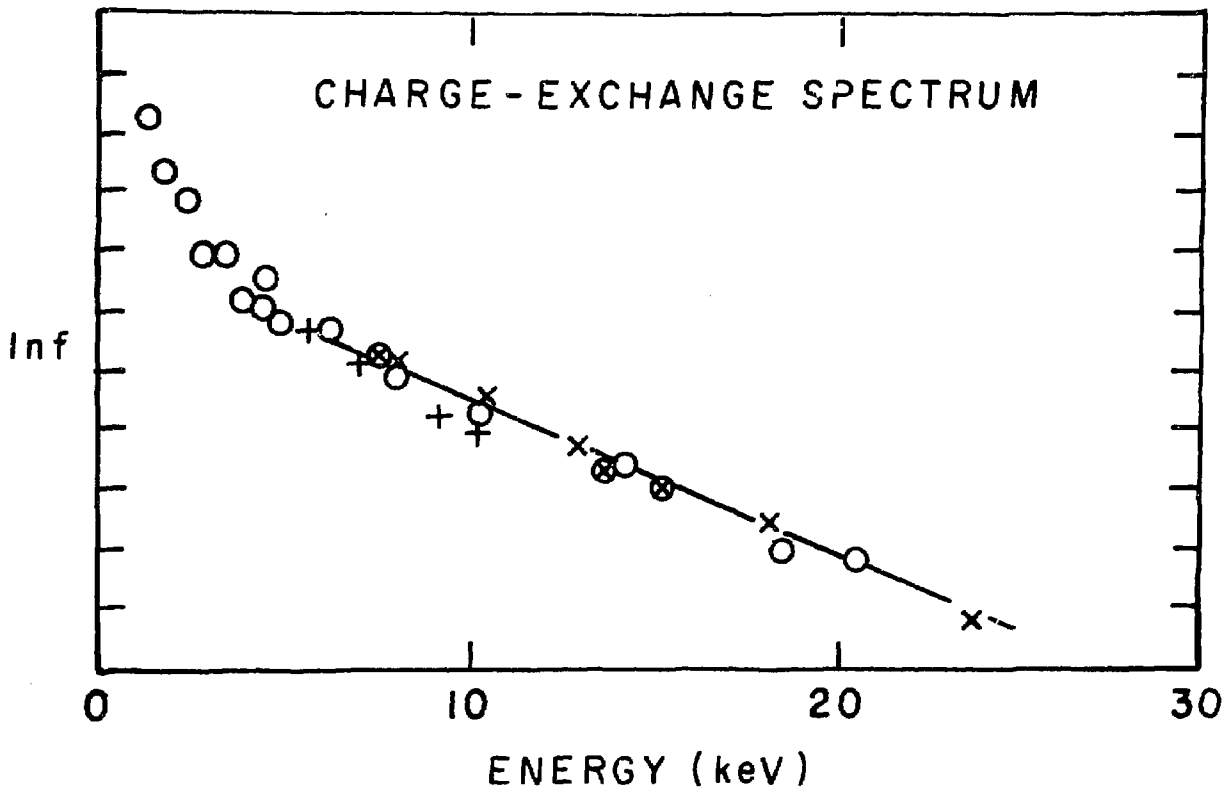

Figure 3. Charge exchange neutral energy distribution. The linear fitting is over an energy range from 1.5 kT_i to 6 kT_i. (PPPL-782883)

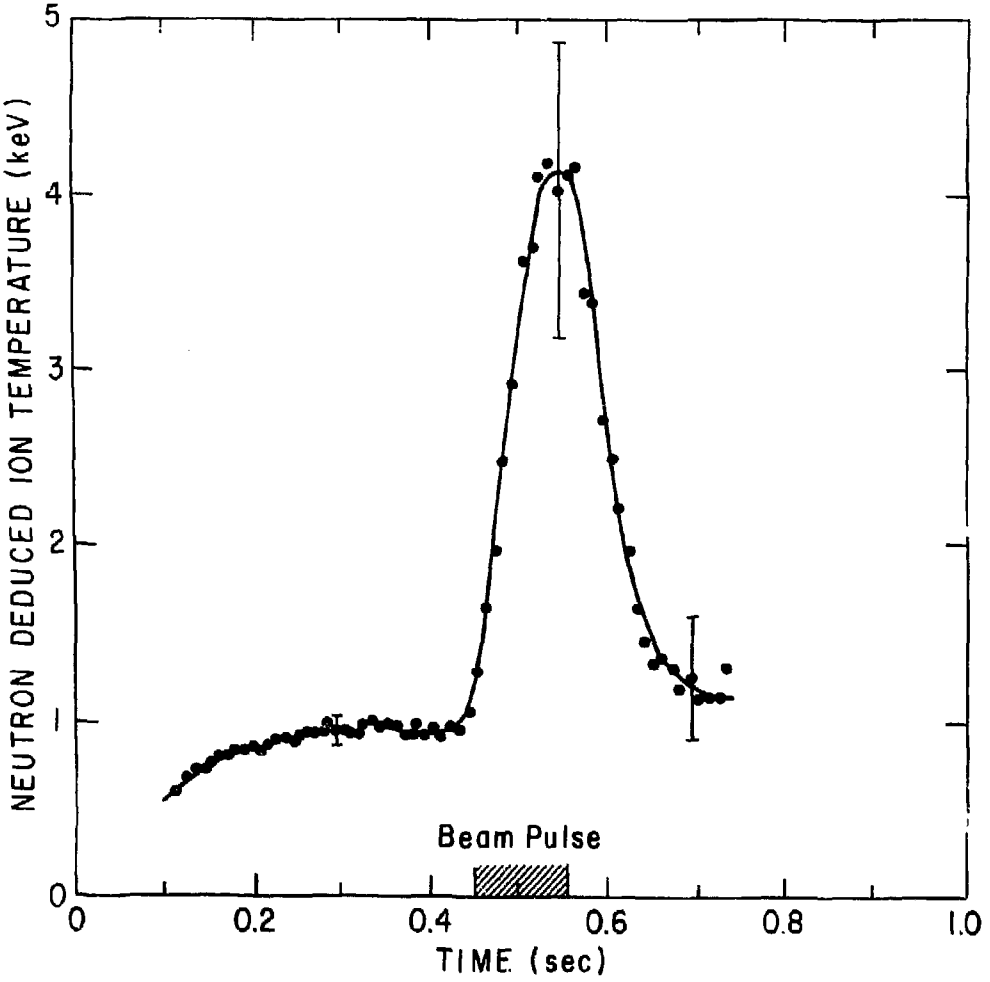

Figure 4. Ion temperature deduced from the neutron emission for the case of 1.4 MW hydrogen beam injection into a deuterium plasma. The neutron emission rose from 5×10^{8} to 4×10^{11} n/sec during the beam heating. (PPPL-7838)

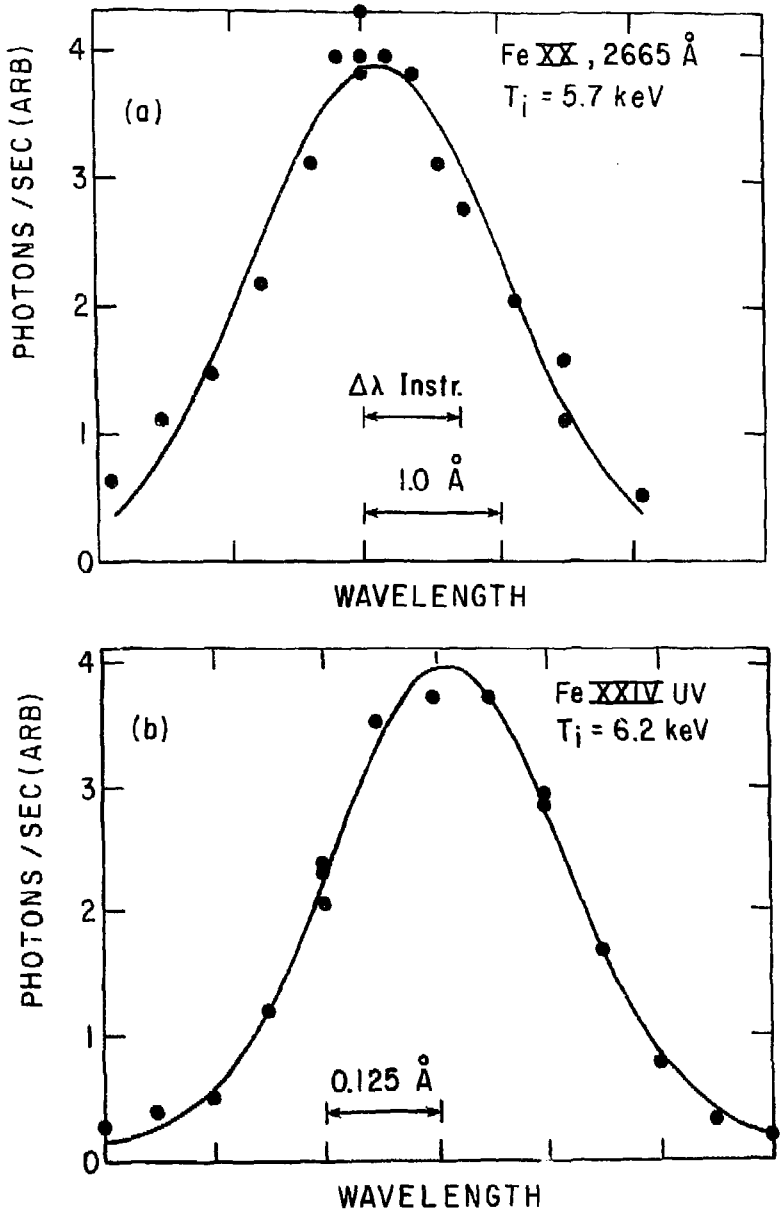

Figure 5. (a) Measured spectral profile of Fe XX 2665 Å line (at t = 550 msec). (b) Measured spectral profile of Fe XXIV 255 Å line (at t = 550 msec). Instrumental width 0.216 A. (PPPL-783884)

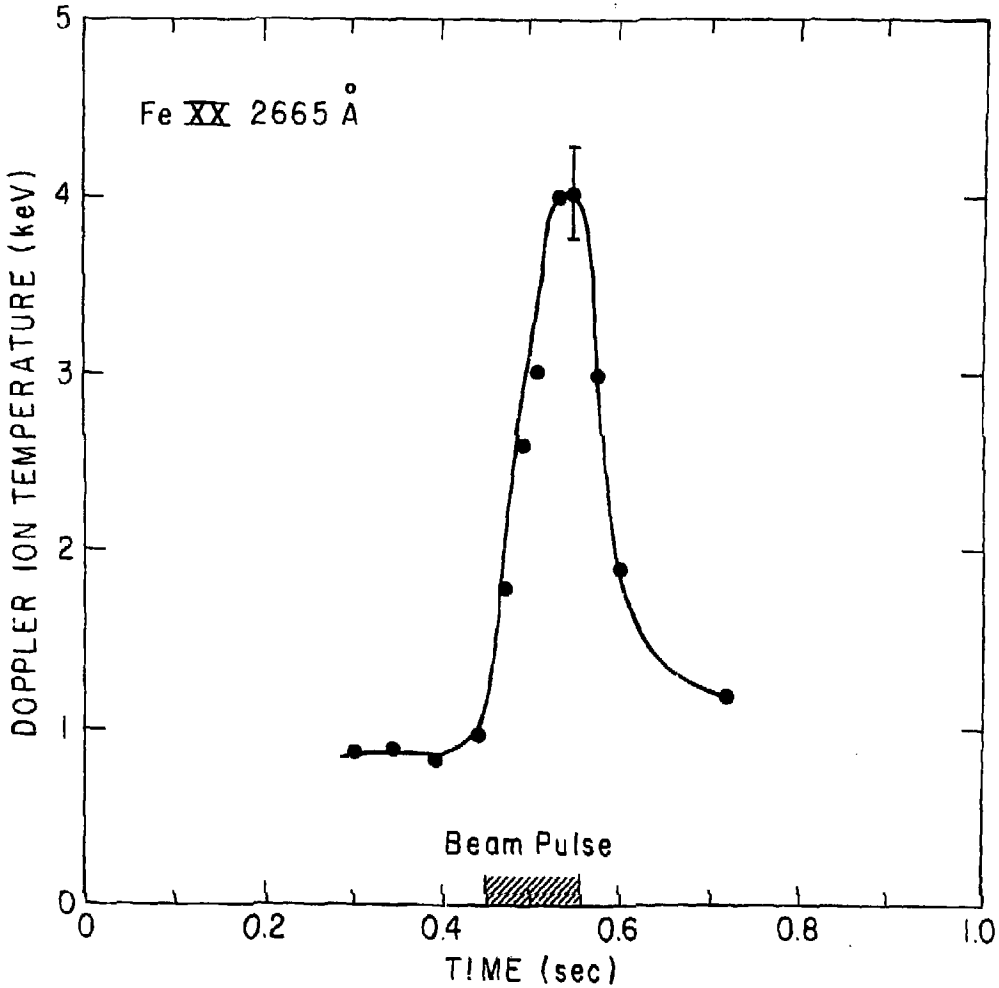

Figure 6. Time evolution of near central ion temperature from Doppler broadening of Fe XX 2665 Å line during P ≈ 1.6 MW neutral beam injection ($H^0 \rightarrow D^+$)
(PPPL-783874)

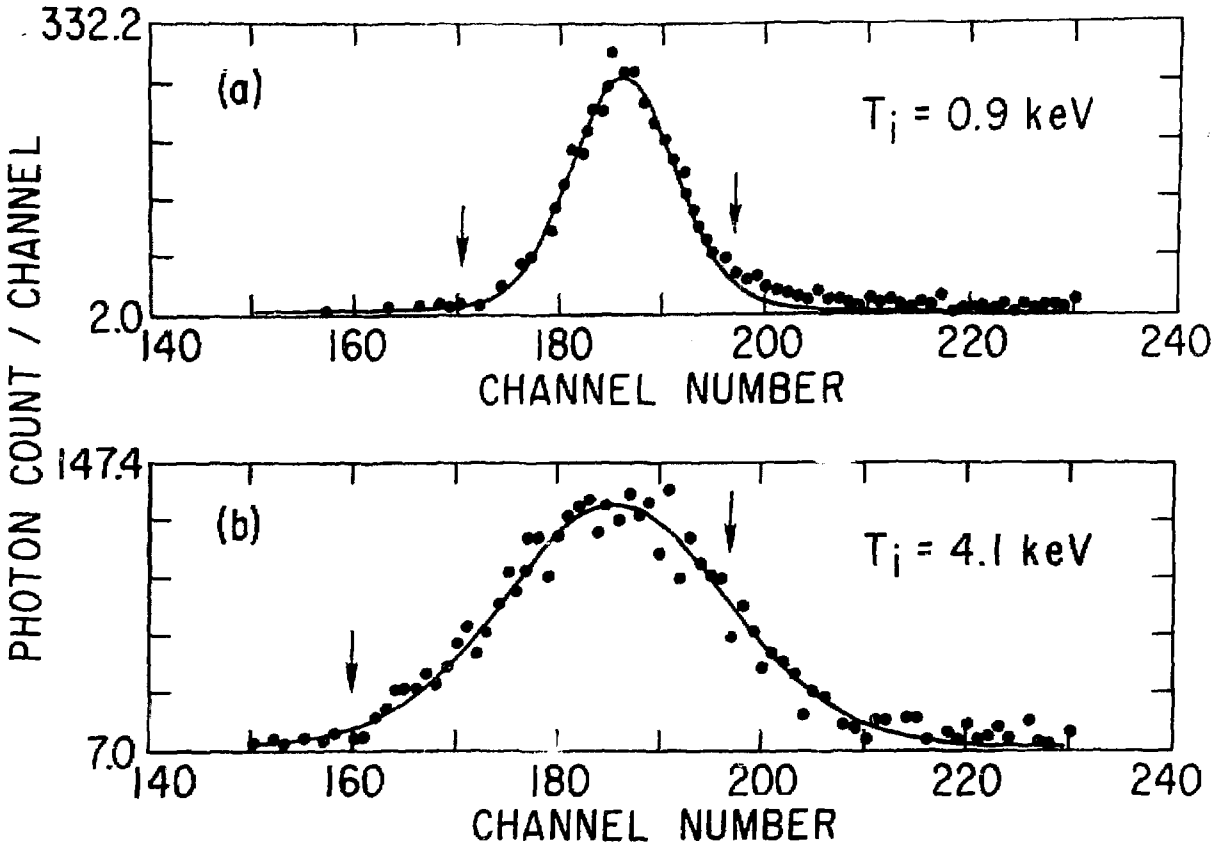

Figure 7. Fe XXV $1s^2(^1S)$-$1s2p(^1P^0)$ line profiles before and during neutral injection. In order to determine the ion temperature, Voigt-functions are fitted to the data. Shown are curve fits for times (a) .425 and (b) .525 sec of Fig. 8. The arrows indicate the fitting region. The conversion gain is .18 eV/channel. The line is centered at 6700 eV. (PPPL-783909)

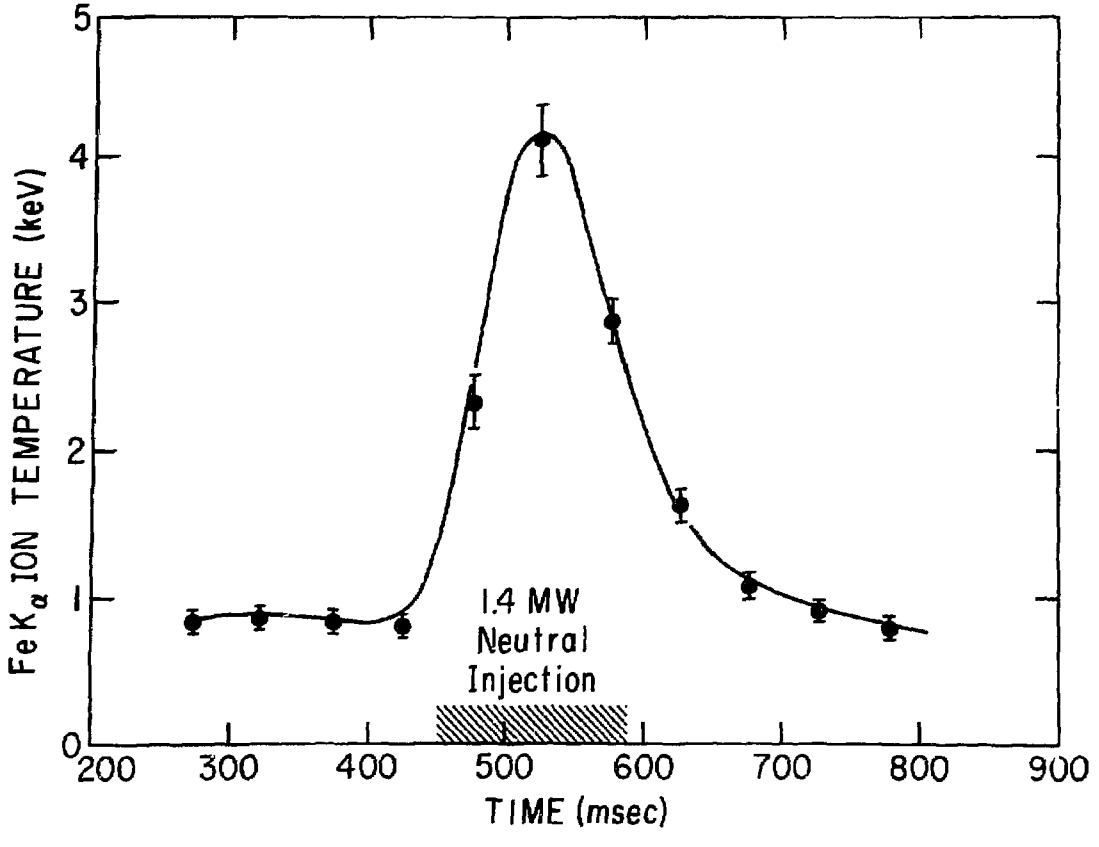

Figure 8. The ion temperature derived from Doppler broadening of the Fe XXV 1.85 Å line during neutral injection. Each point is taken over an integration time of 50 msec. (PPPL-783871)

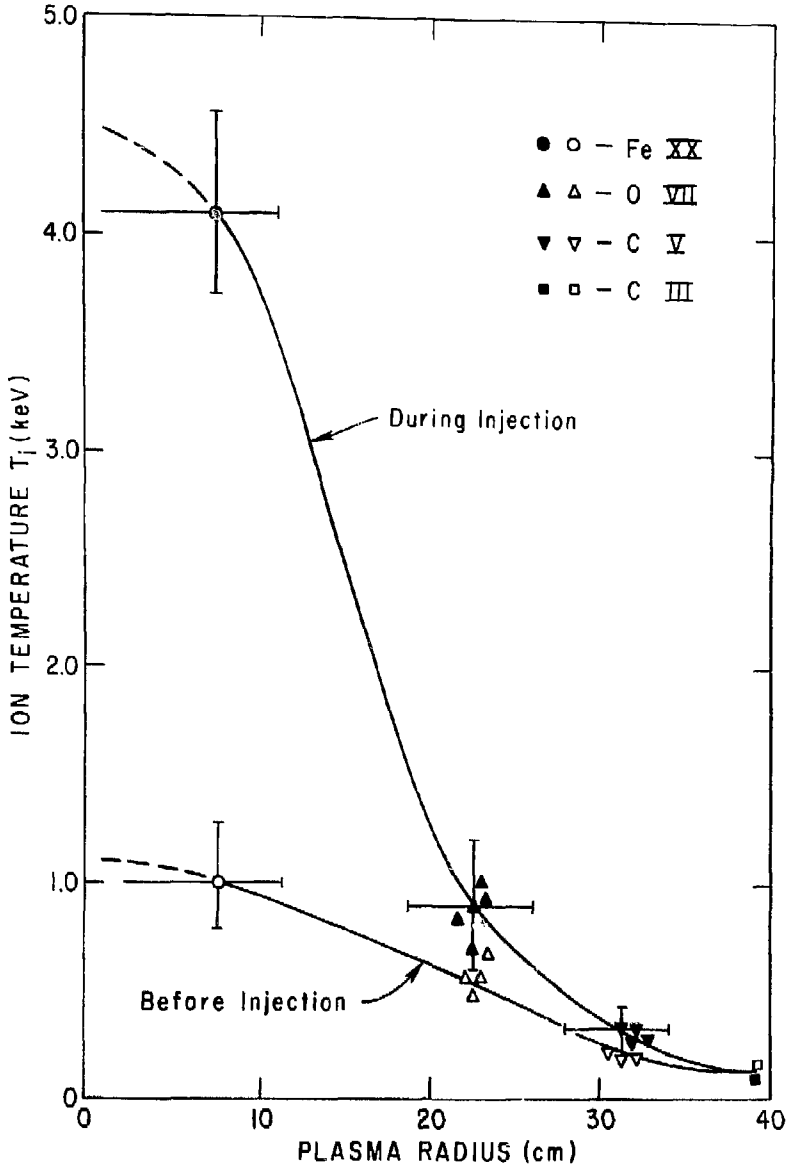

Figure 9. Radial profile of ion temperature before and during neutral beam injection ($H^0 \rightarrow D^+$; P ≈ 1.6 MW) from Doppler broadening of Fe XX 2665 Å, OVII 1623 Å, CV 2271 Å and CIII 2237 Å lines. (PPPL-783878)

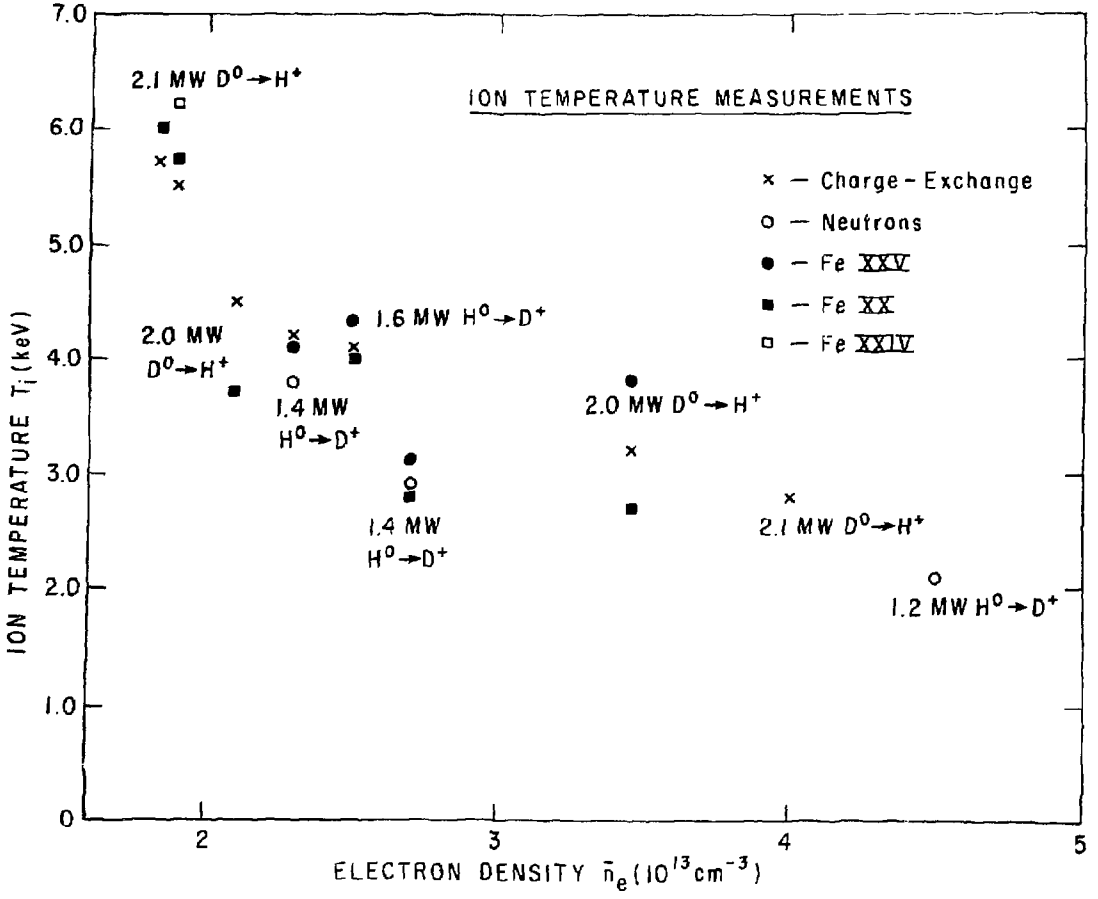

Figure 10. Ion temperature measurements vs line average electron density for four beam operation, carbon limiters and titanium gettering. (PPPL-783864)

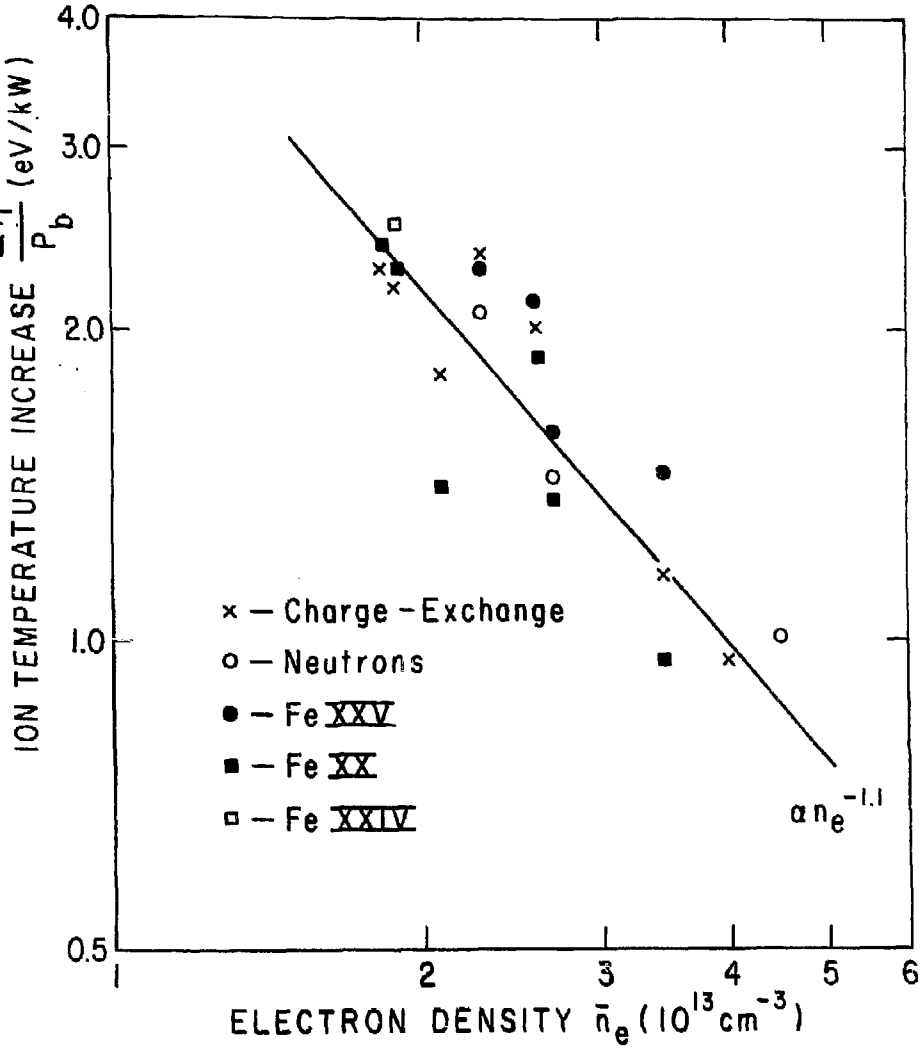

Figure 11. Scaling of ion temperature measurements vs. line average electron density. (PPPL-783866)

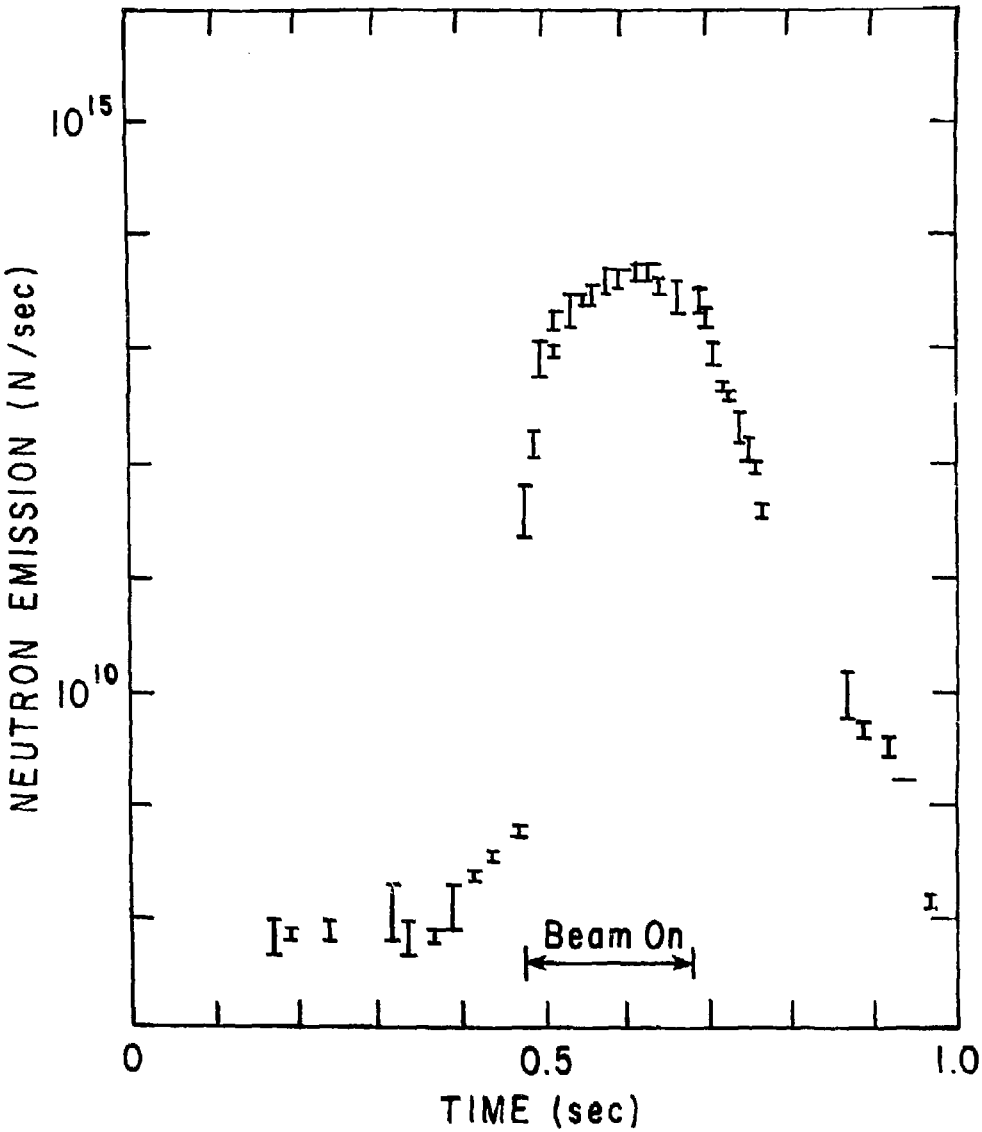

Figure 12. Beam induced neutron emission for the case of 1.7 MW deuterium beam injection into a deuterium plasma. The peak intensity is 4×10^{13} n/sec and the total yield is 7×10^{12} neutrons/shot. (PPPL-783875)

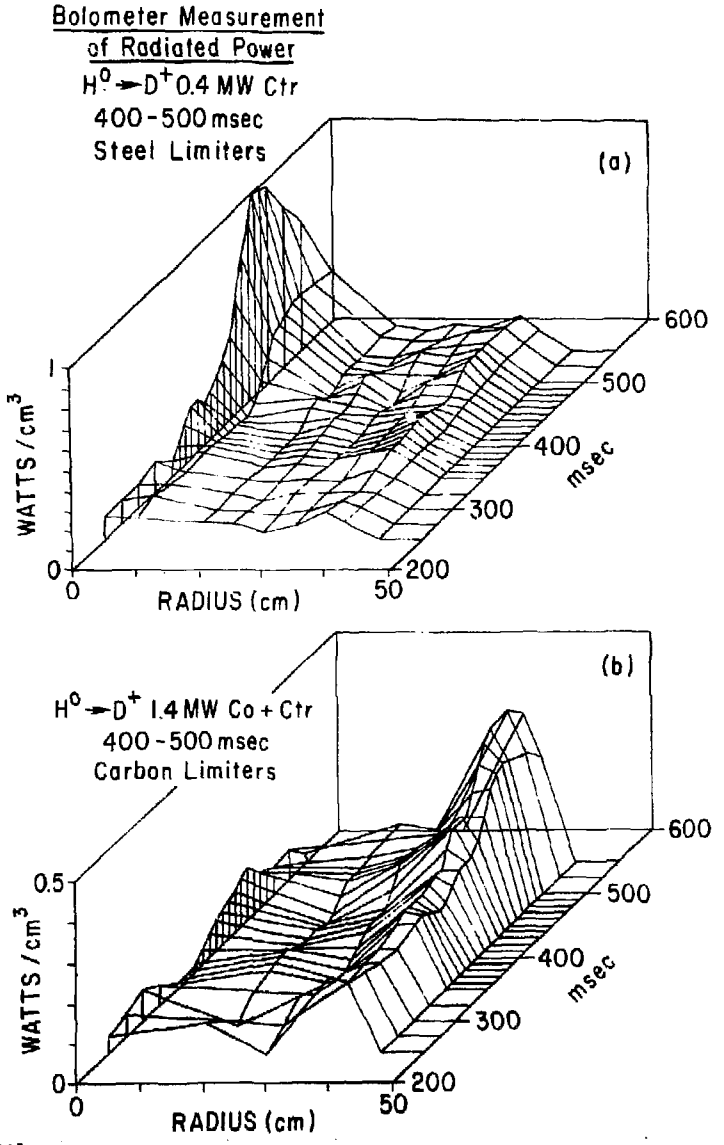

Figure 13. Bolometric measurement of the radiated power as a function of radius and time. (a) The deuterium target plasma is characterized by $\bar{n}_e = 2.7 \times 10^{13}$ cm^{-3} [$n_e(0) = 5 \times 10^{13}$ cm^{-3}], $T_e(0) = 1.4$ keV, $I_p = 380$ kA. $V_p = 1.5$ volts, with steel limiters, and Ti gettering at the wall. One hydrogen neutral beam is injected in the counter direction between 400 and 500 msec with 0.4 MW. (b) The deuterium target plasma is characterized by $\bar{n}_e = 2.8 \times 10^{13}$ cm^{-3} [$n_e(0) = 5 \times 10^{13}$ cm^{-3}], $T_e(0) = 2$ keV. $I_p = 450$ kA, $V_p = 1.3$ volts, with water-cooled carbon limiters, and Ti gettering at the wall. Four hydrogen neutral beams co- and counter- are injected between 400 and 500 msec with a total power of 1.4 MW.

(PPPL-783869)

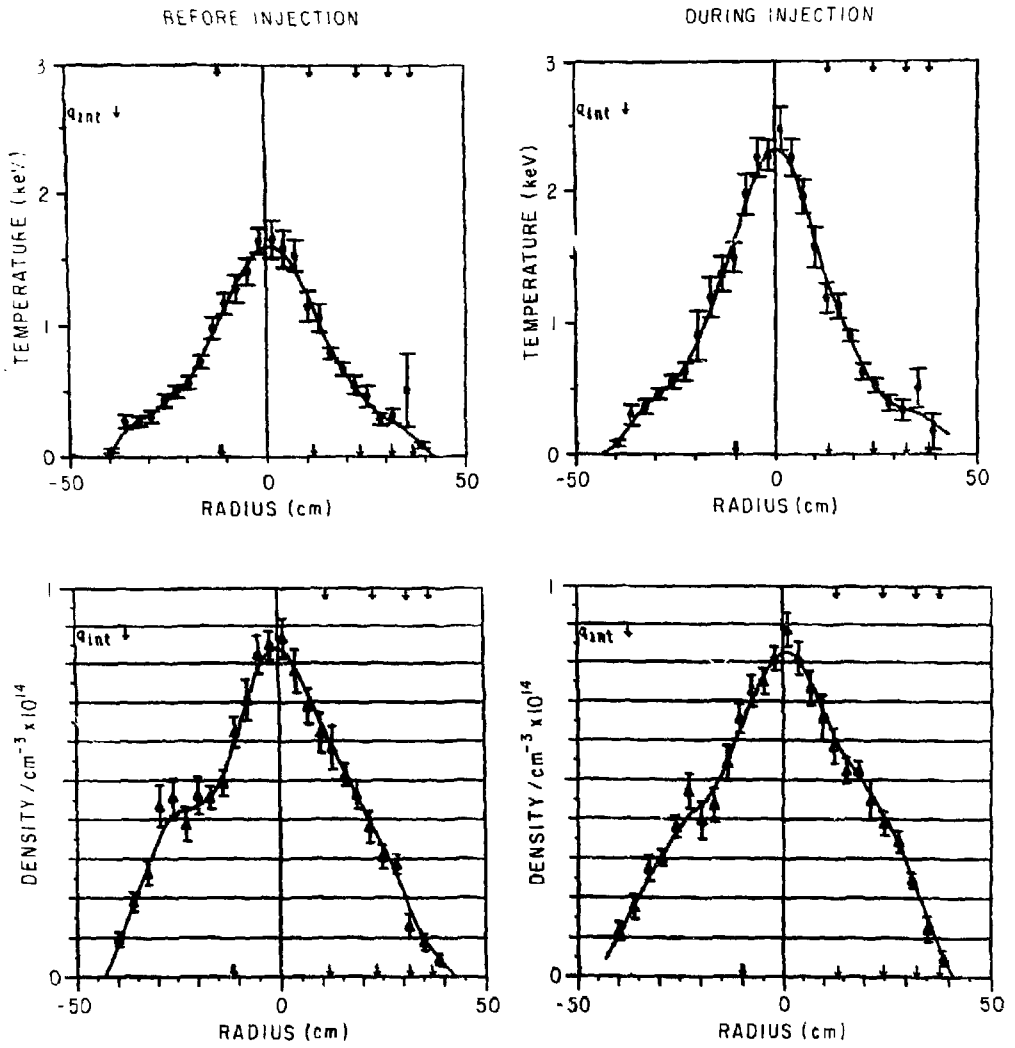

Figure 14. Single shot electron temperature and electron density profiles from Thomsor scattering. Error bars on the points are determined from least squares fit to the scattered spectrum at each radial position. Solid line through the points is a spline fit tothe data. Arrows indicate integral q surface positions. (PPPL-783870)

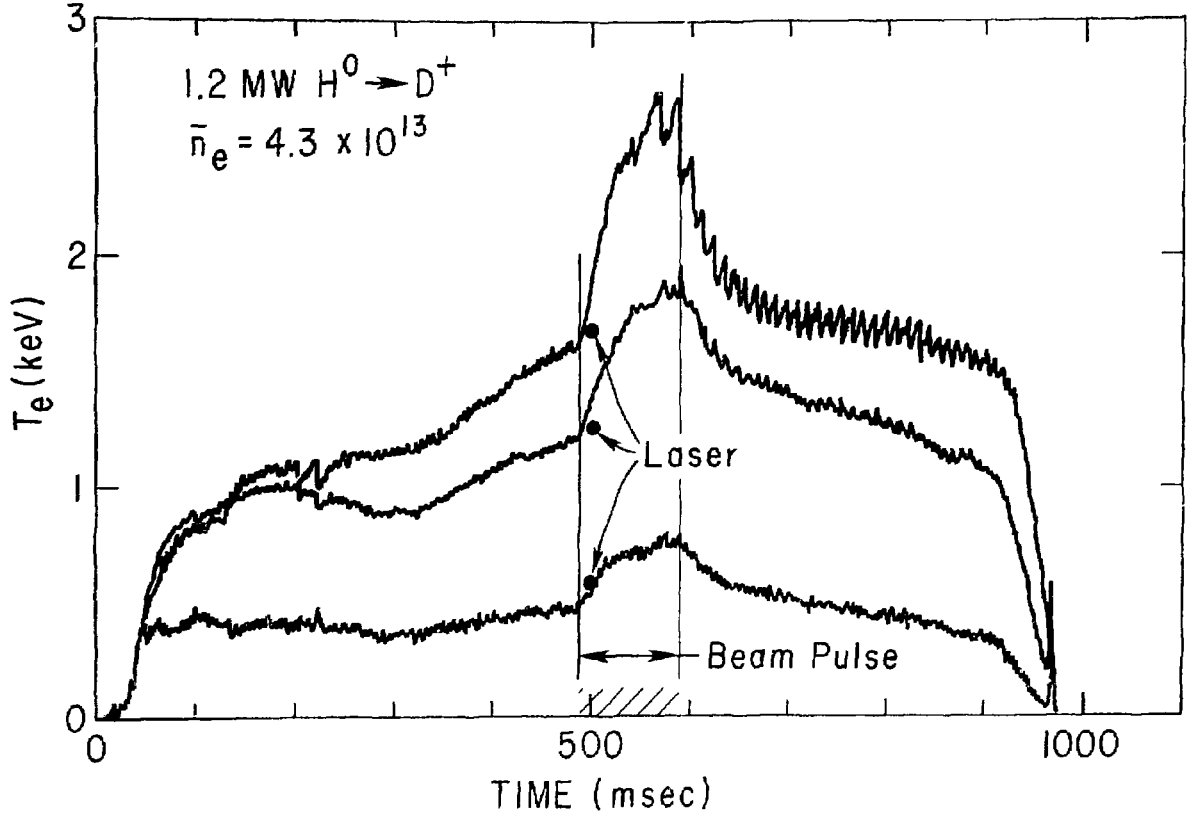

Figure 15. Electron temperature as a function of time for three radial positions. This information is provided by a grating polychromator which analyzes second harmonic electron cyclotron radiation. Substantial electron heating is produced by the injection of three neutral hydrogen beams of total power 1.2 MW into the deuterium plasma ($\bar{n}_e = 4.3 \times 10^{13}$ cm^{-3} at the end of the beam pulse). For the same shot and radial positions, the temperatures obtained at a single point in time with the TV Thomson scattering system are indicated. (PPPL-783902)

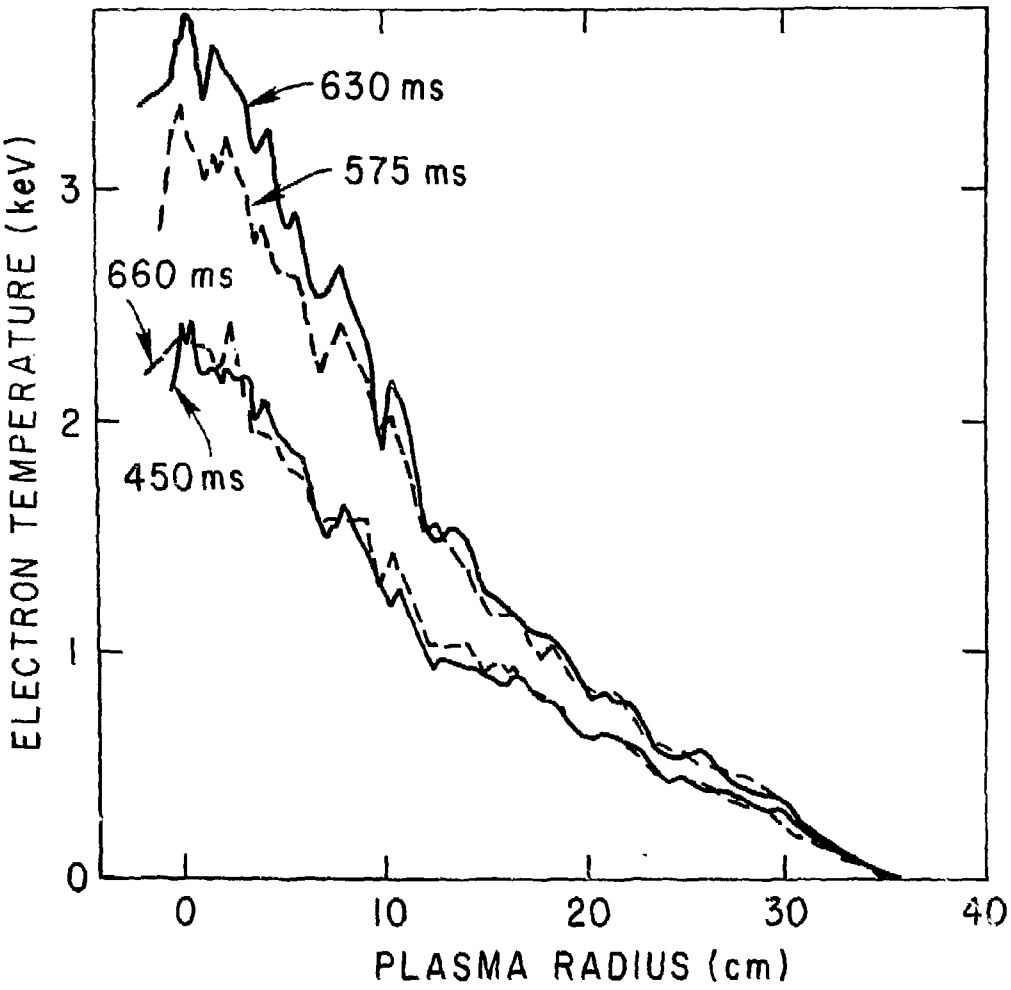

Figure 16. The electron temperature profile before, during and after injection of 2.1 MW deuterium neutral beams at time t = 450-600 ms into a low density ($\bar{n}_e = 1.8 \times 10^{13}$ cm^{-3}) hydrogen plasma. The observed peaking of the electron temperature profile 30 ms after the termination of injection can be explained by heating of the electrons by the still energetic slowing-down ions and the removal of the power loss due to the thermalization of cold electrons incoming with the beam ions. These profiles were ascertained from the fundamental electron cyclotron emission measured by a fast-scanning heterodyne receiver. (PPPL-783904)

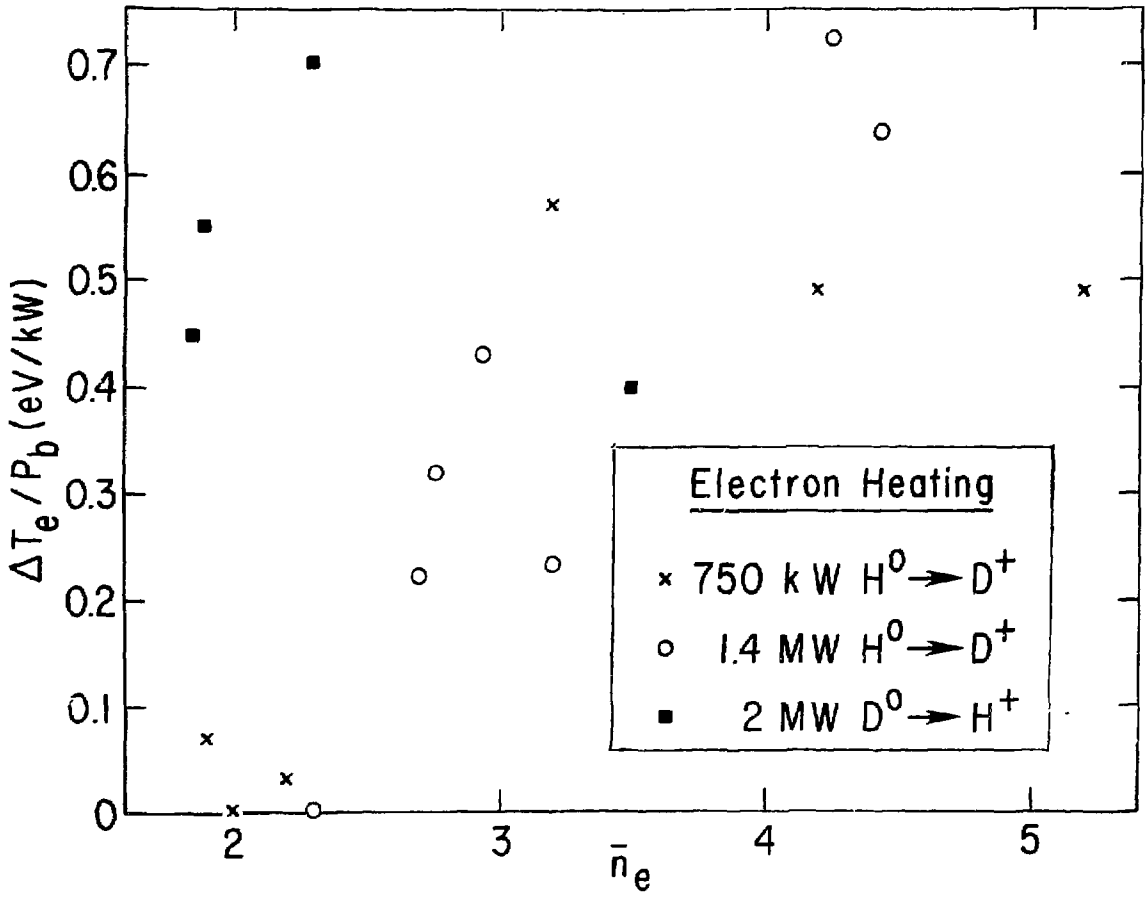

Figure 17. Compilation of the results of high power injection into gettered carbon limiter plasmas. The overall picture suggests that under the best conditions $\Delta T_e/P_b \approx 0.6$ eV/kW, independent of plasma density. (PPPL-783908)

PLT INJECTION ANALYSIS

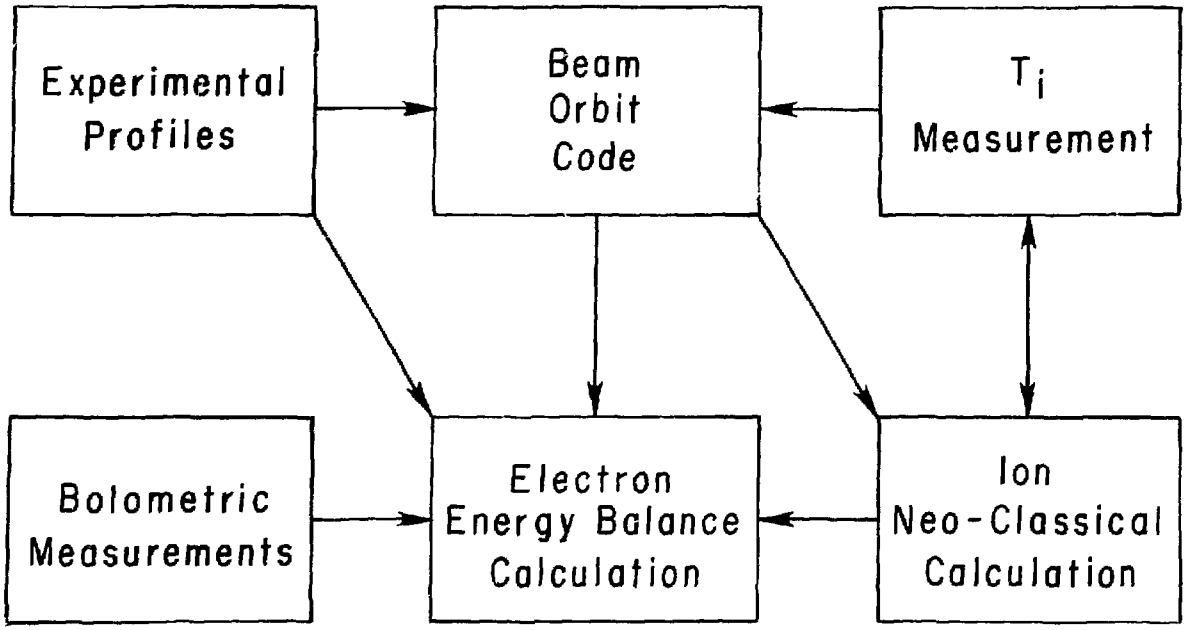

Figure 18. Logical structure of ion and electron power balance calculations. (PPPL-783868)

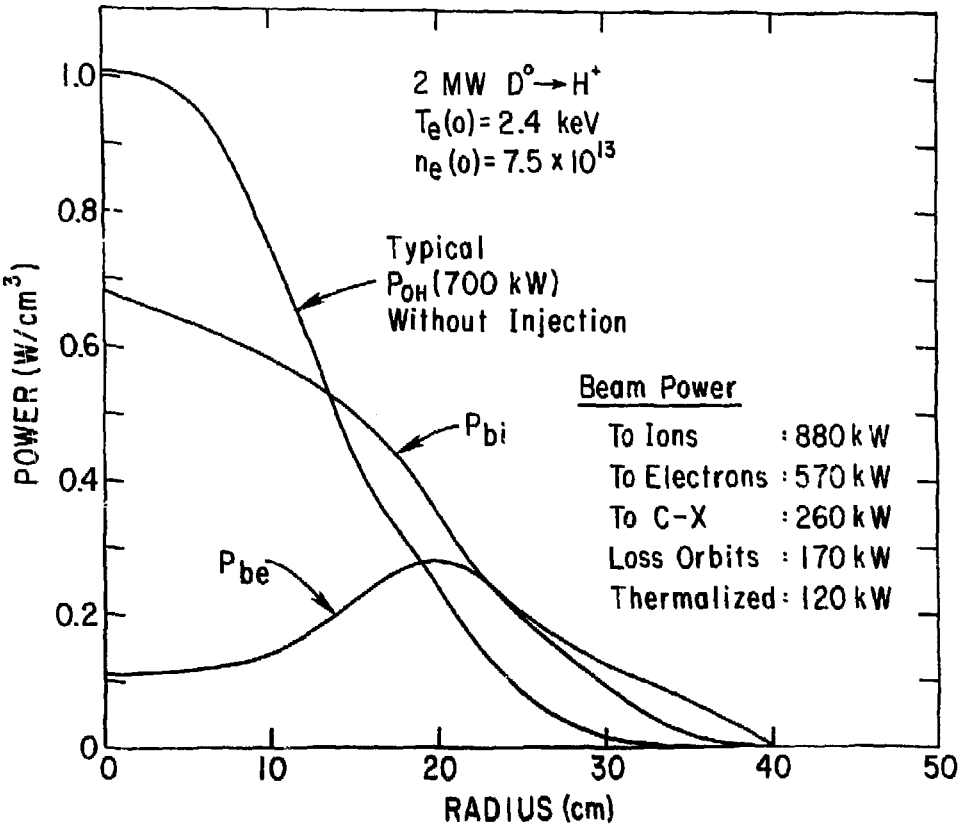

Figure 19. Beam power deposition profiles from Monte Carlo beam-orbit code. (PPPL-783901)

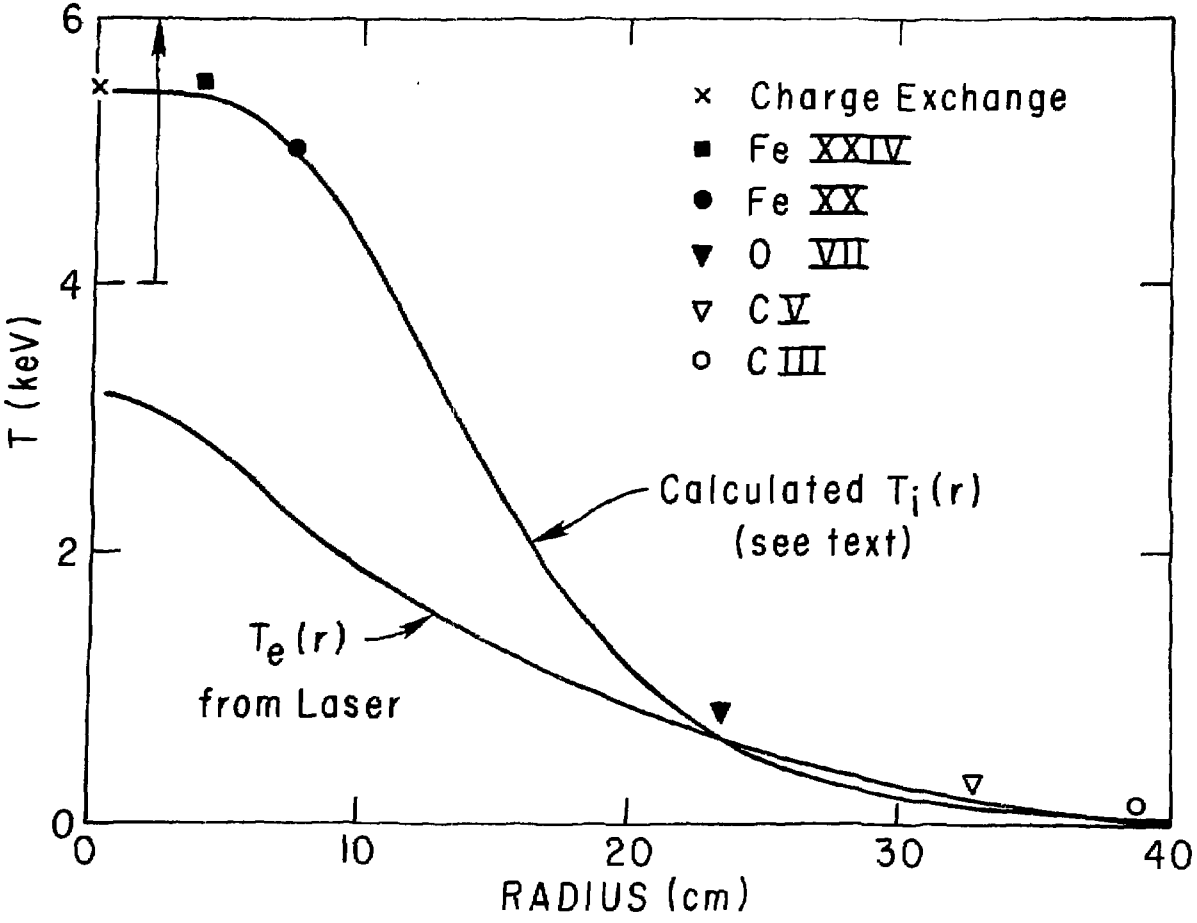

Figure 20. Calculated ion temperature profile with central value calibrated to experimental data, 2.1 MW D° injection into low density H^+ plasma.
(PPPL-783893)

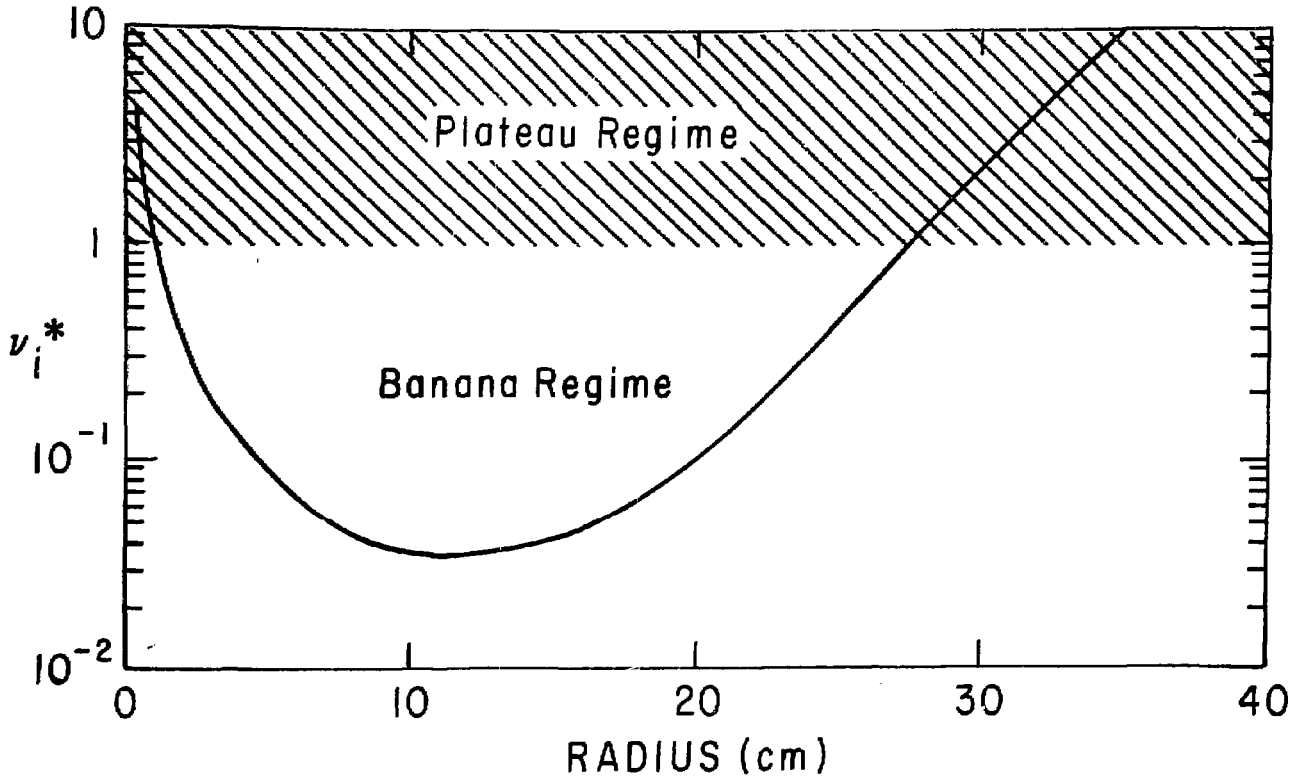

Figure 21. Calculated ion collisionality (solid curve) for ion temperature profile shown in Fig. 20. (PPPL-783895)

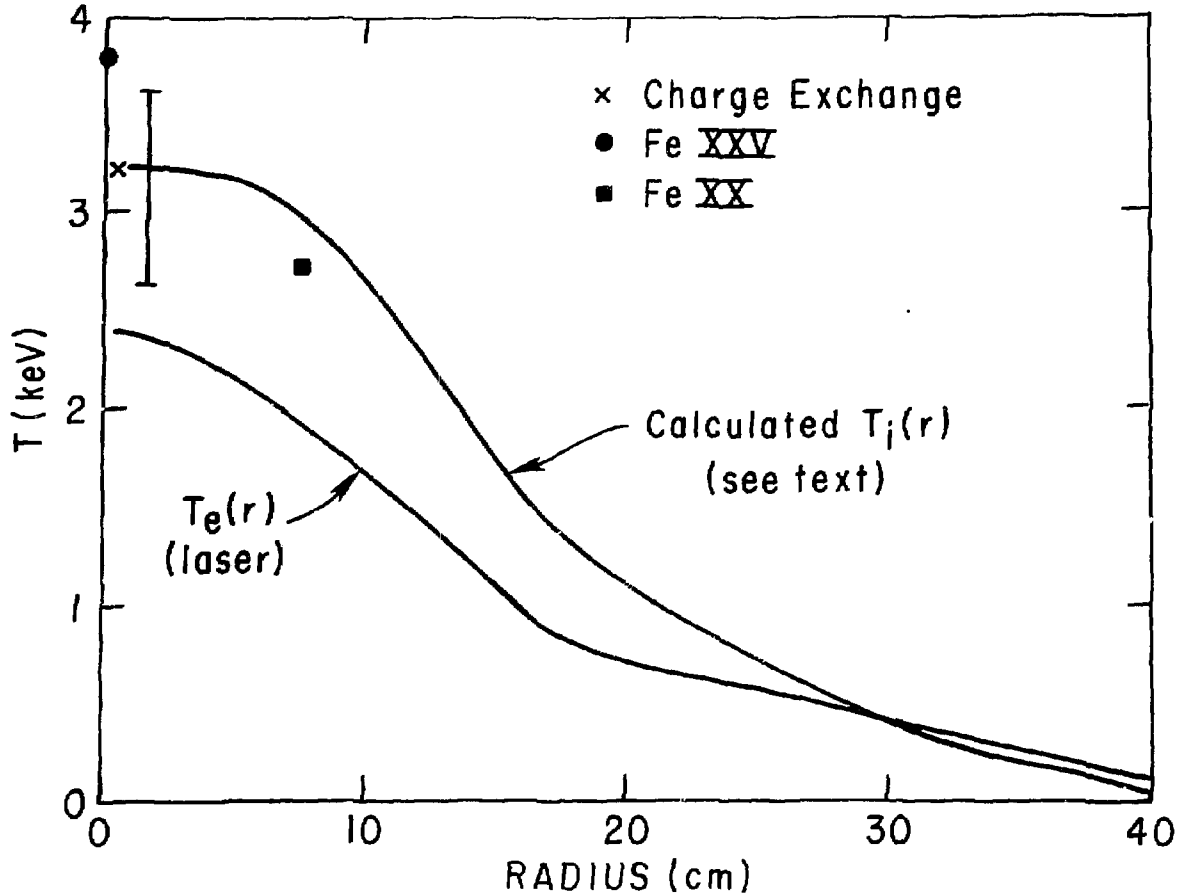

Figure 22. Calculated ion temperature profile with central value calibrated to experimental data. 2.0 MW D° injection into moderate density H^+ plasma. (PPPL-783900)

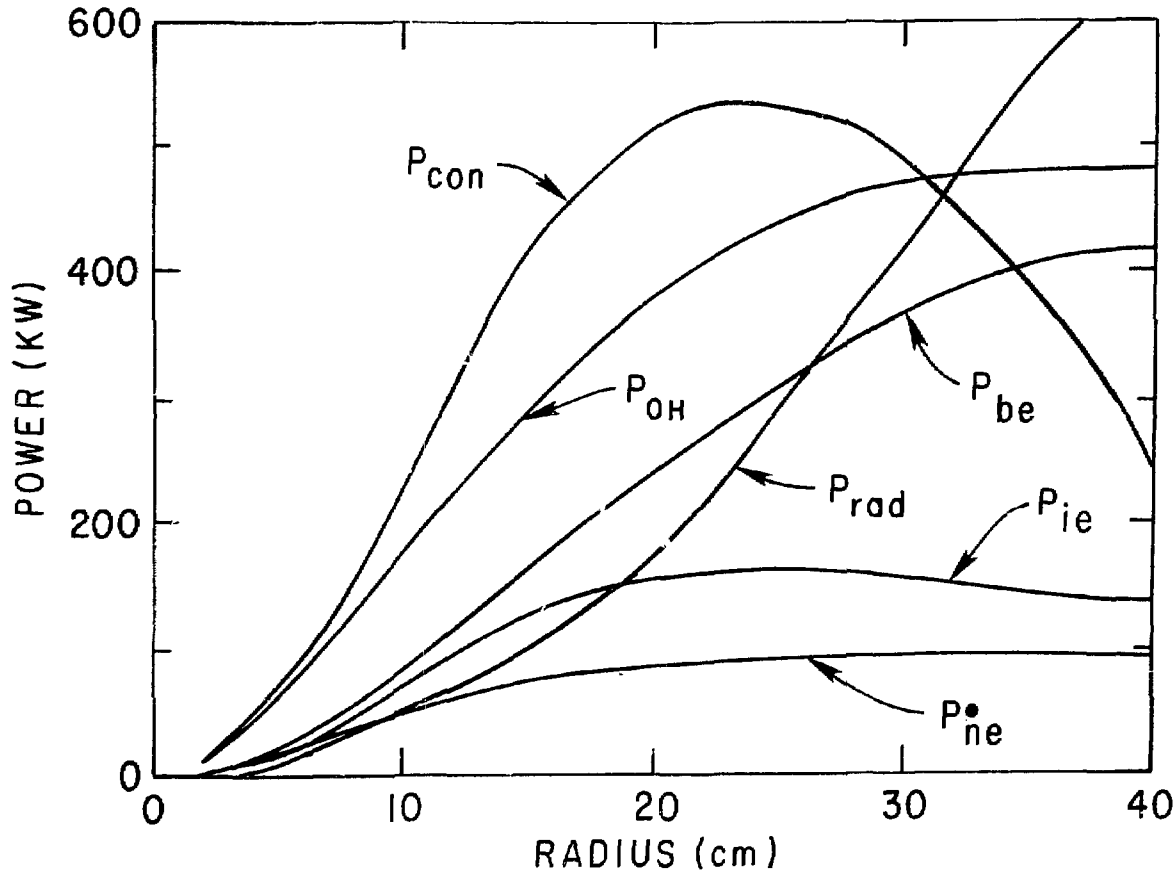

Figure 23. Radial electron power flows for 2.1 MW D° injection into low density H^+ plasma. (PPPL-783898)

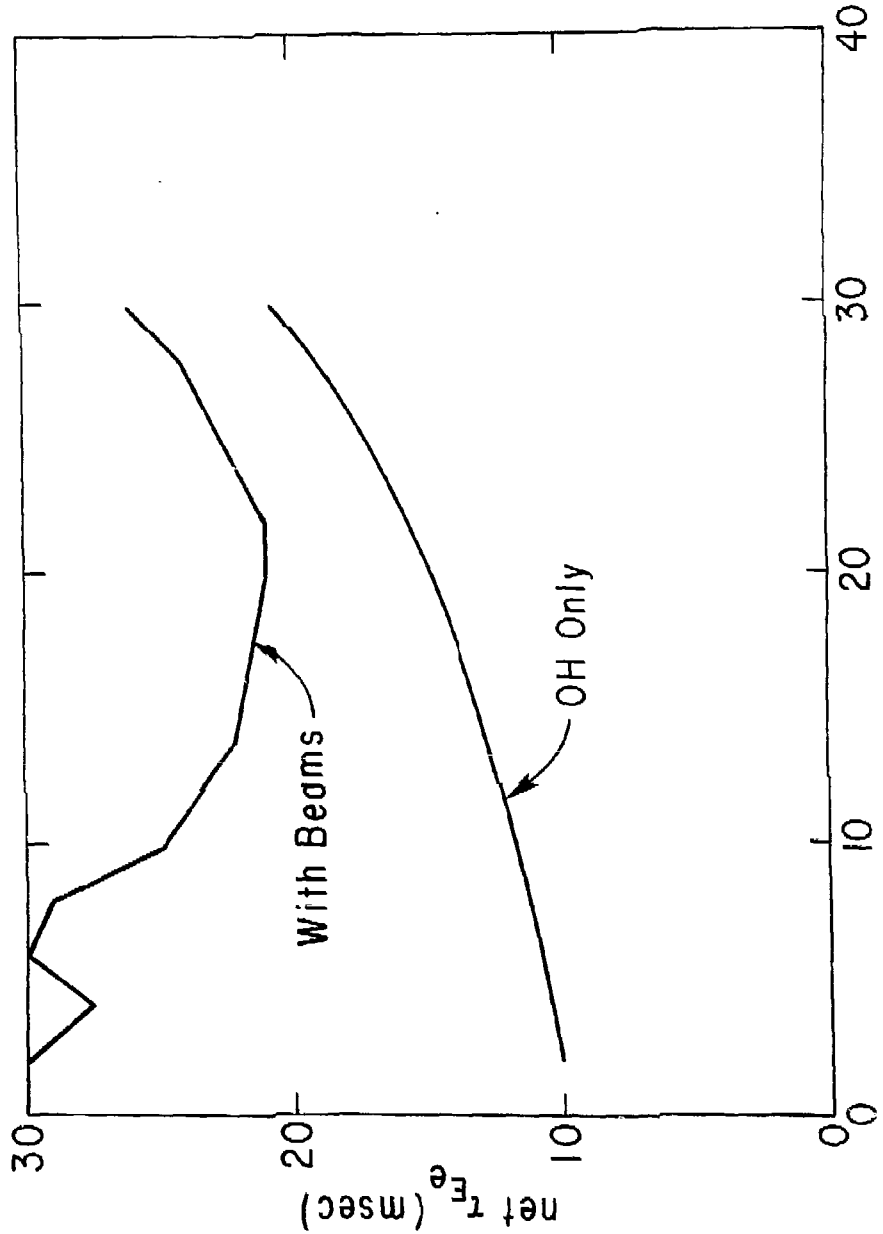

Figure 24. Radially integrated net τ_{Ee} for 2.1 MW D° injection into low density H^+ plasma. (PPPL-783907)

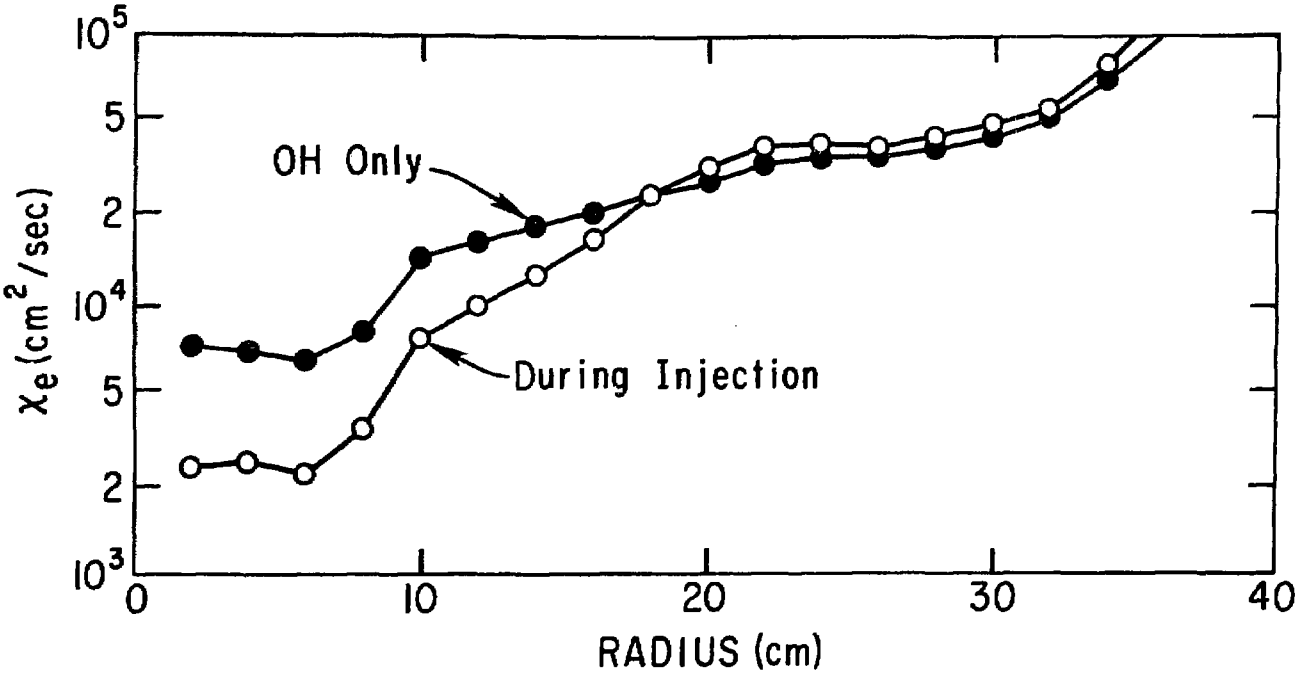

Figure 25. $\chi_e(r)$ calculated from experimental temperature and density profiles and radial electron power flows. (PPPL-783914)

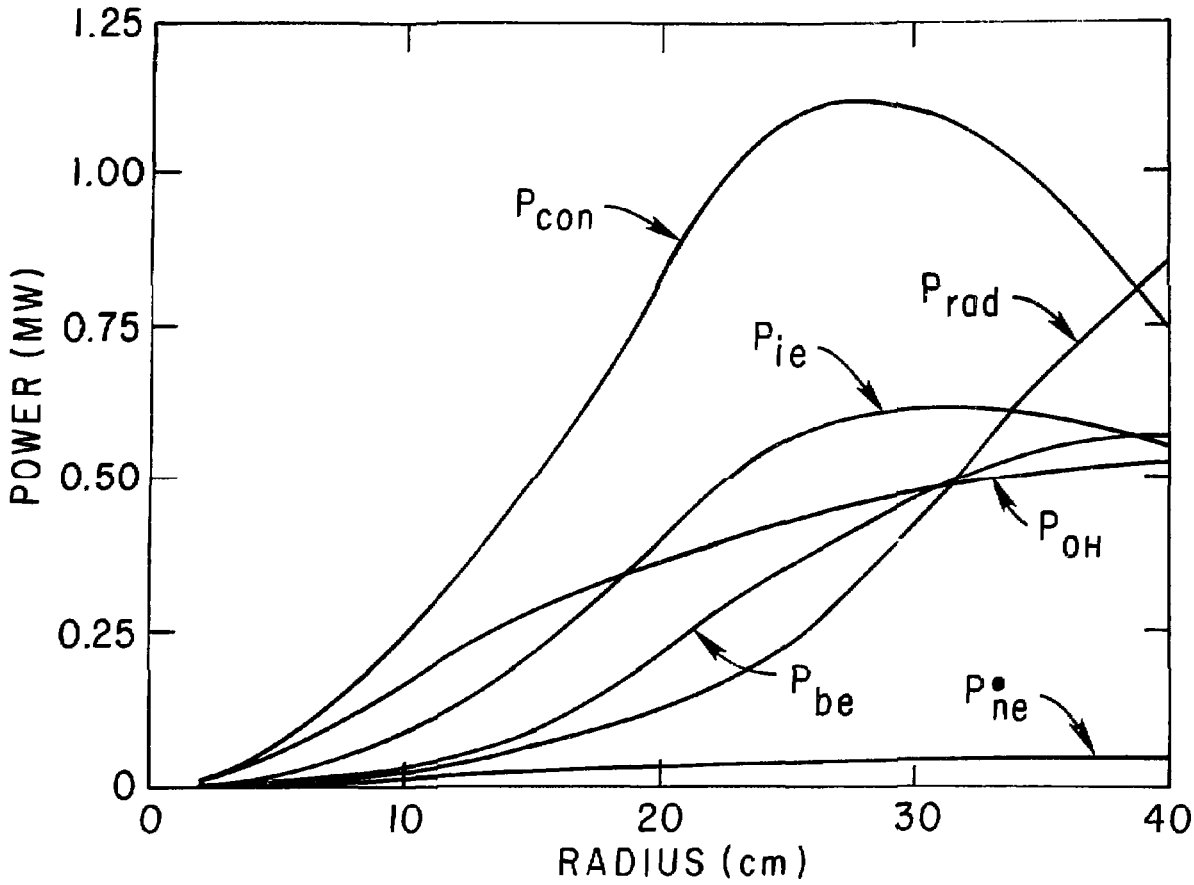

Figure 26. Radial electron power flows for 2 MW D° injection into moderate density H^+ plasma. (PPPL-783896)

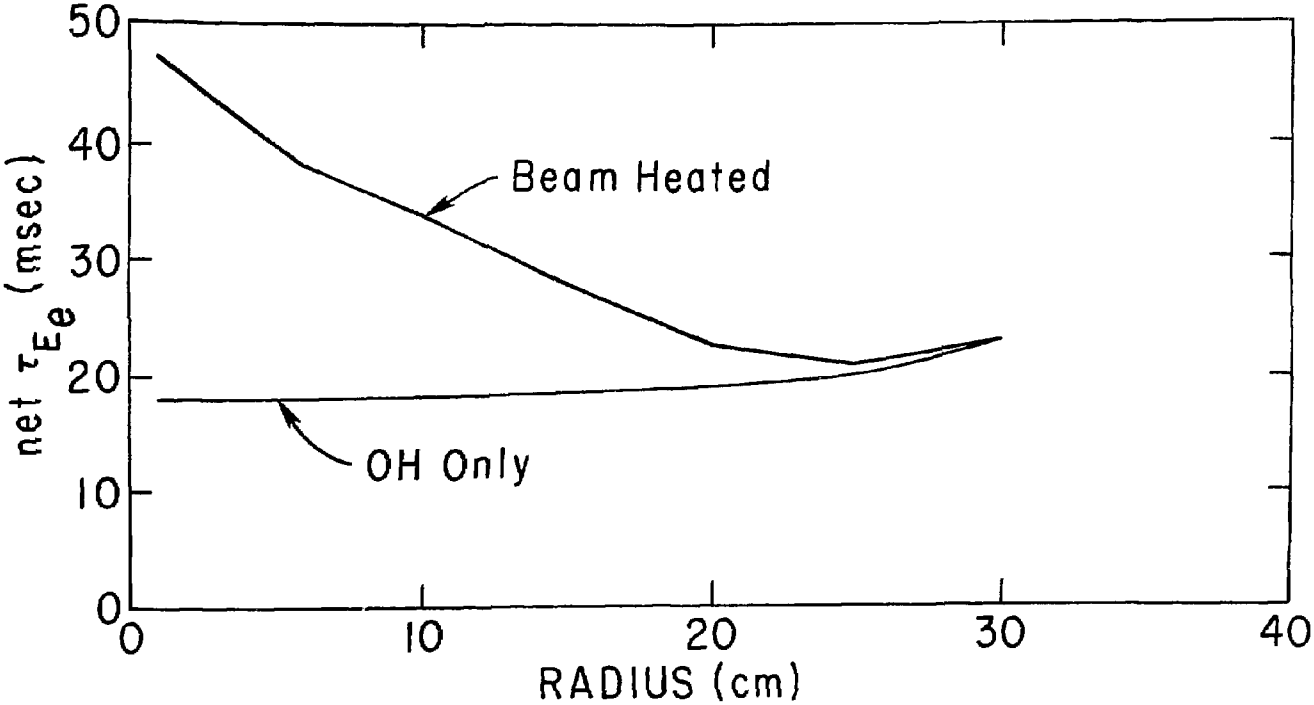

Figure 27. Radially integrated net τ_{Ee} for 2 MW D° injection into moderate density H^+ plasma. (PPPL-783913)

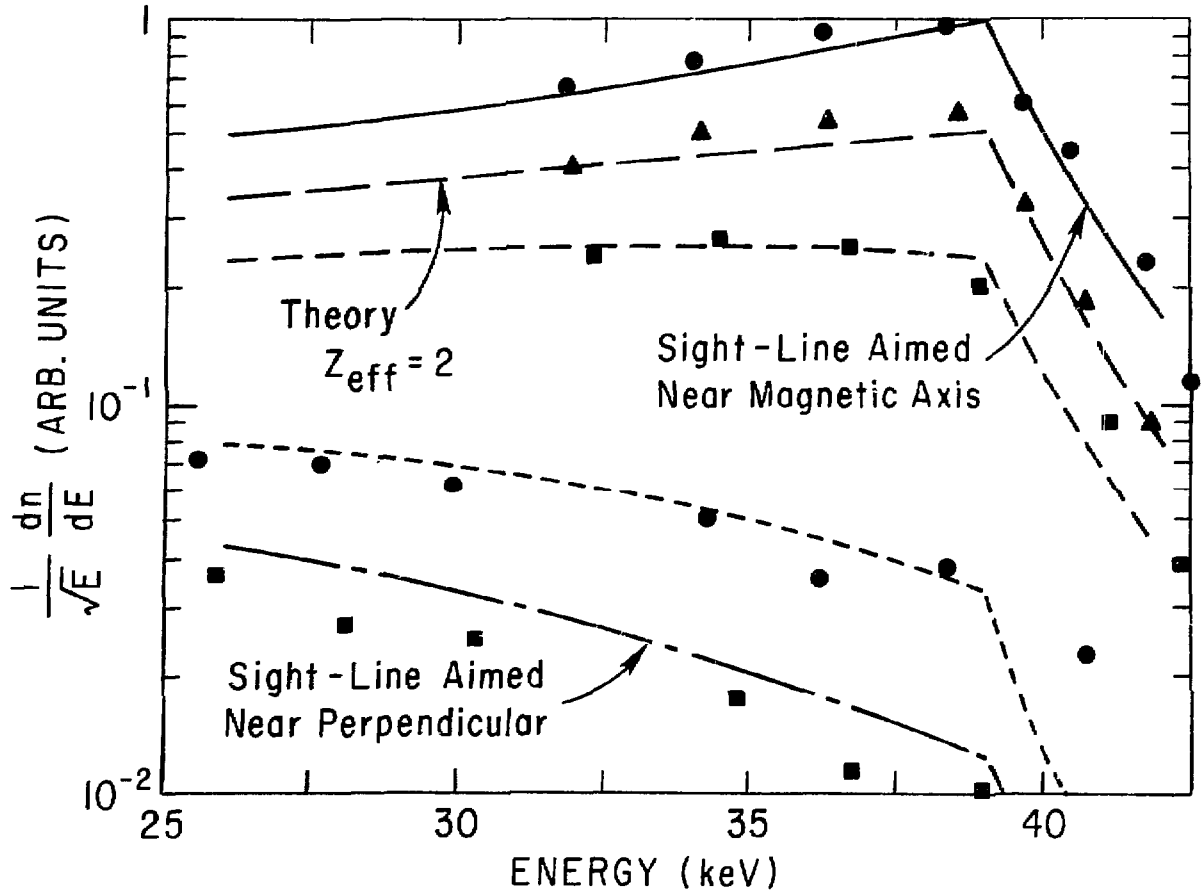

Figure 28. Energy spectra of fast neutrals emitted from the plasma at a number of different angles; experiment vs. theory. (PPPL-783494)

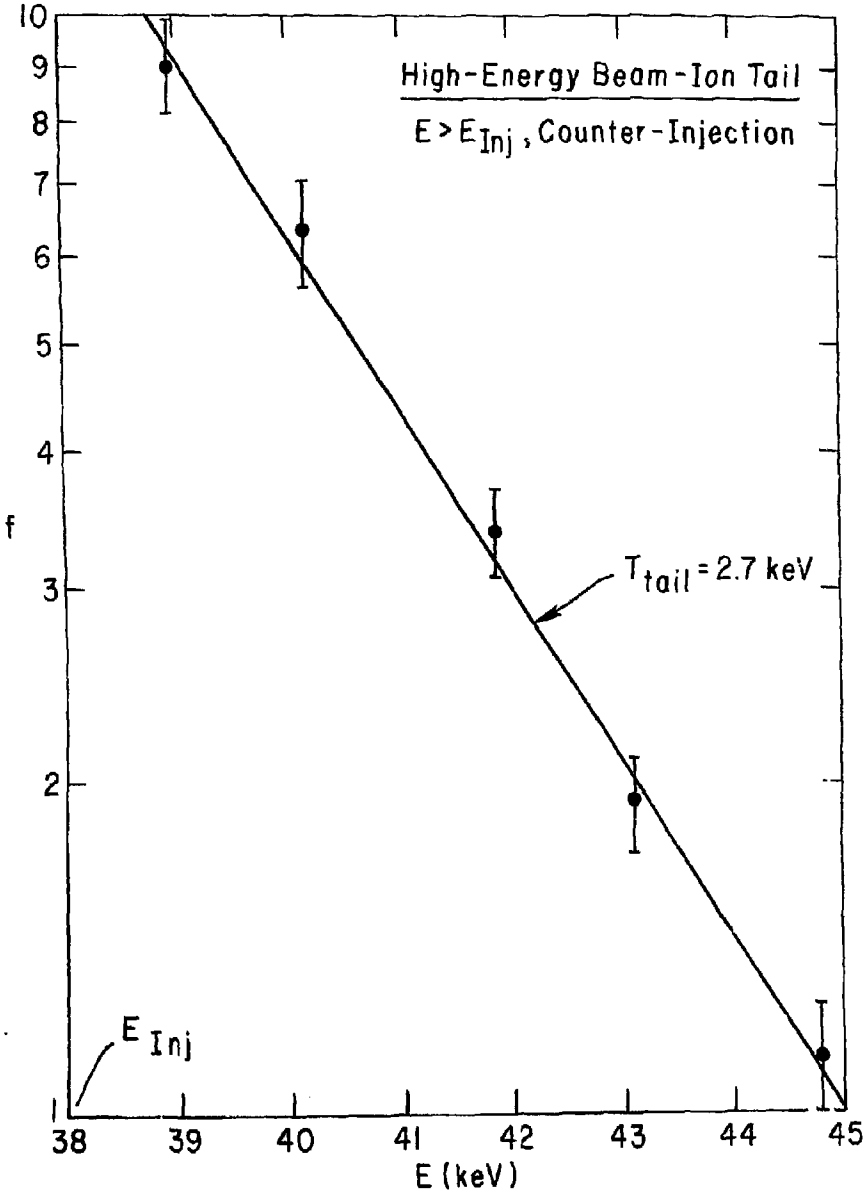

Figure 29. High energy beam-ion tail above the injection energy, analyzer aimed tangentially, facing counter-going ions. (PPPL-783910)

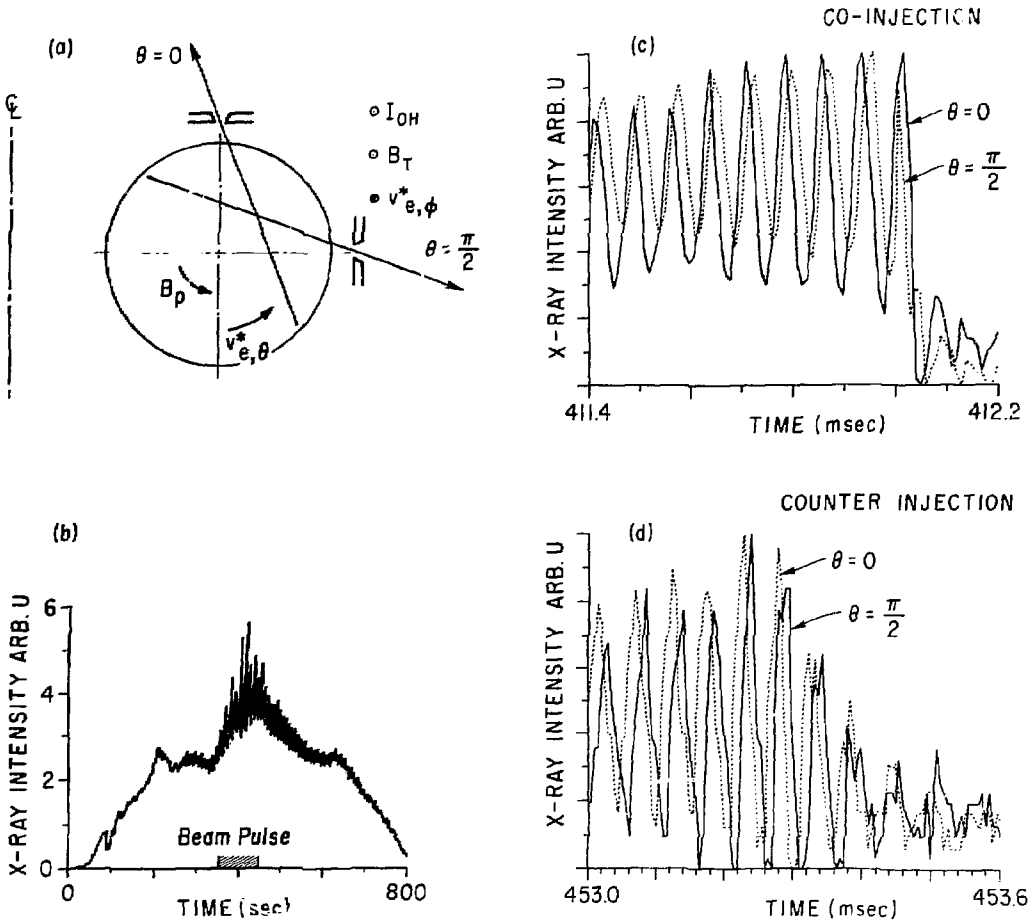

Figure 30. Plasma rotation during neutral beam injection. Large sawtooth oscillations develop during injection (b). The traces from two detectors looking through the plasma along chords $\theta = 0$ and $\theta = \pi/2$ (a) are compared for co-injection (c) and counter-injection (d) indicating propagation in ion and electron diamagnetic direction, respectively. (PPPL-783882)

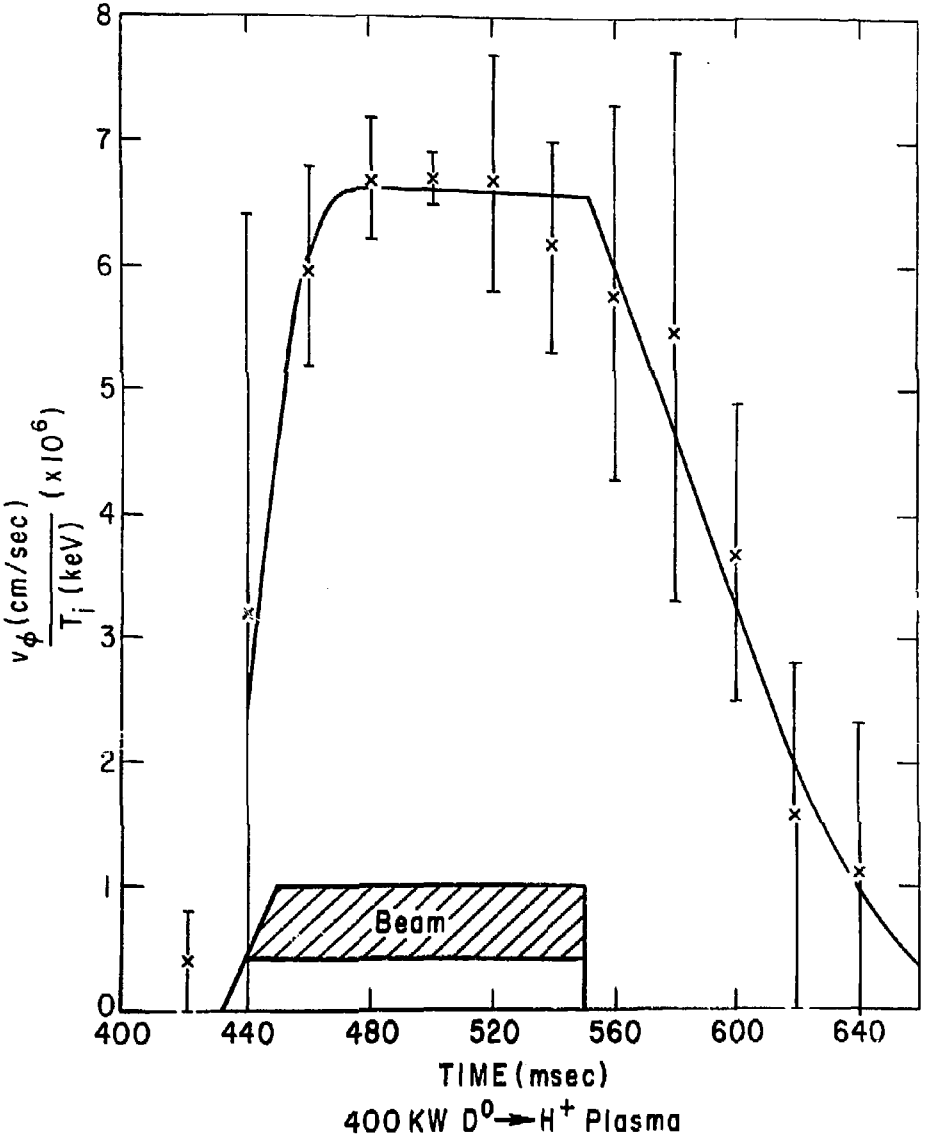

Figure 31. v_ϕ/T_i vs. time deduced from tangential thermal fast neutral flux. (PPPL-783906)

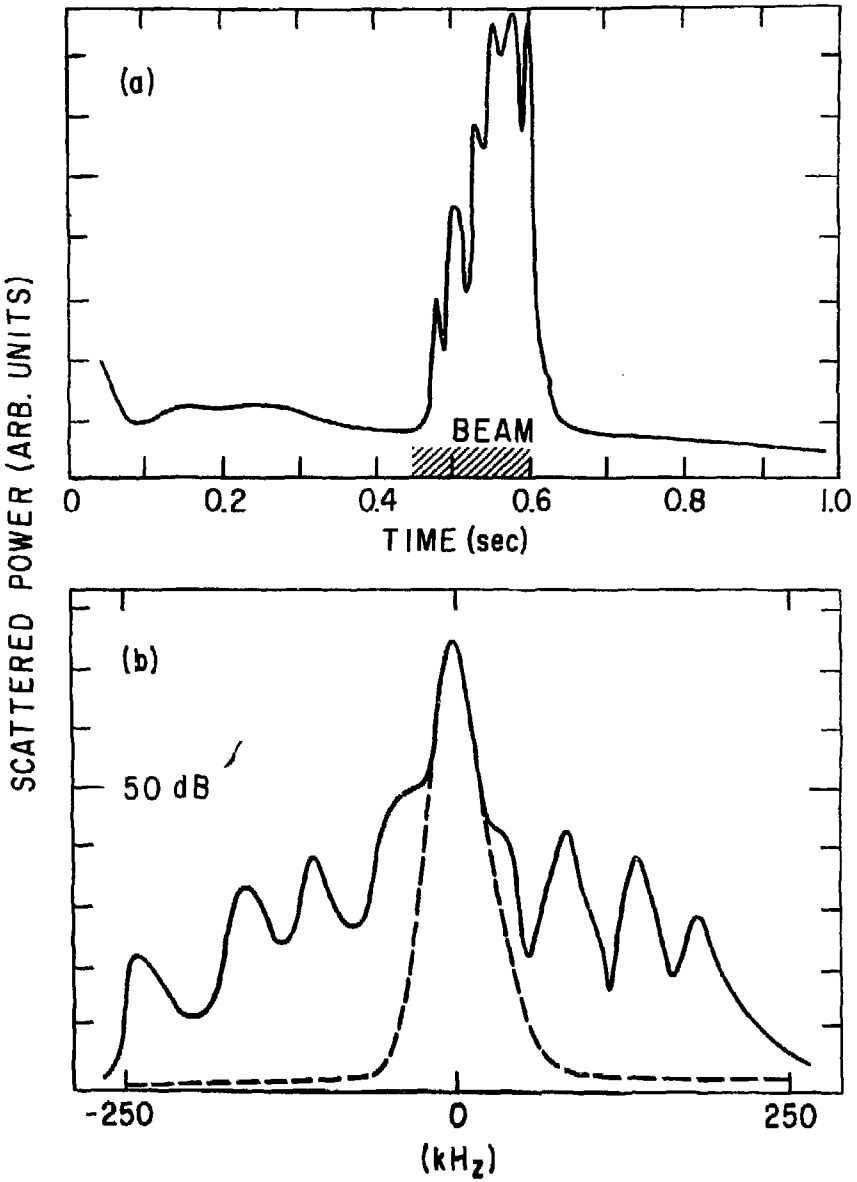

Figure 32. (a) Time behavior of scattered power for a case of 2.1 MW D° injection into low density H^+ plasma. (linear scale) (b) Frequency power spectrum of density fluctuations at t = 550 msec. (dB scale) (PPPL-783867)